Marine Geology 459 (2023) 107032

Contents lists available at ScienceDirect

Marine Geology

journal homepage: www.elsevier.com/locate/margo

Research Article

A multi-proxy approach to assess tsunami hazard with a preliminary risk assessment: A case study of the Makran Coast, Pakistan

Rashid Haider [a,d,*], Sajid Ali [b], Gösta Hoffmann [c], Klaus Reicherter [a]

[a] Institute of Neotectonics and Natural Hazards, RWTH Aachen University, Lochnerstr. 4-20, 52056 Aachen, Germany
[b] COMSATS University Islamabad, Abbottabad campus, Department of Earth Sciences, Pakistan
[c] UNESCO Global Geoparks Unit, Department Heritage, Nature, Ecology, German Commission for UNESCO, Martin-Luther-Allee 42, 53175 Bonn, Germany
[d] Geoscience Advanced Research Laboratories, Geological Survey of Pakistan, Islamabad 45500, Pakistan

ARTICLE INFO

Editor: Edward Anthony

Keywords:
Tsunami hazard
Inundation analysis
Makran subduction zone (MSZ)
Multi-proxy approach

ABSTRACT

Tsunamis and cyclones are sea-borne hazards capable of inundating vast coastal areas. This study aims at an extreme wave hazard assessment with a preliminary inundation analysis along the Makran Coast, Pakistan. The coastal hazard, particularly tsunamis, is evaluated by integrating five approaches: (i) probabilistic tsunami hazard assessment (PTHA), (ii) deterministic tsunami hazard assessment (DTHA), (iii) geophysical-seismic (2-D seismic) modelling, (iv) sedimentary tsunami deposits (tsunamites) and (v) the historical record. The recurrence interval for a mega-tsunami event (>10 m) is between 500 and 1000 years in the Arabian Sea. Of these mega-tsunamis, about 60% are generated by seismic sources, while the remaining 40% are attributed to secondary (co-seismic submarine landslides) and other non-seismic sources. Based on the above five approaches, the hazard analysis helped to shortlist four wave scenarios (3, 7, 10, and 15 m), which were further used to demarcate risk areas through static inundation analysis. The results indicated that the damage potential at the coast is minor to negligible with 3 m waves and moderate with 7 m waves, whereas the 10 m and 15 m waves will severely damage the study area. In addition to tsunami risk, cyclone risk is assessed by incorporating storm tracks dating back to 1945 CE. In the last 64 years, cyclone frequency has jumped from 2 cyclones per 15 years to 10 cyclones per 15 years, and the intensity has increased by two levels from Tropical Storm (TS) to Category-3.

1. Introduction and aims

Tsunamis, cyclones and rising sea levels are natural hazards to coastal areas. In the Indian Ocean, the 1970 Bhola cyclone in the Bay of Bengal, the 1998 Gujarat cyclone in the Arabian Sea, and the 2004 tsunami along Sumatra Island are some of the major catastrophic events that resulted in >0.5 million casualties and more than USD 14 billion in property loss (Frank and Husain, 1971; Kalsi and Gupta, 2003; Ball, 2011[illegible]). In spite of such huge losses, the lessons learned from these events are not widely anticipated on the mitigation side (Latcharote, 2017). In this regard, the Makran Coast of Pakistan is also poorly prepared, as the life and property losses during the 1945 tsunami and the cyclones of 1998, 1999, 2007, 2010 and 2021 reflect a dejected level of preparedness and resilience. Along the coastline of Pakistan, >24 million people are exposed to these hazards (see Fig. 1). Another point of concern is the Karachi Nuclear Power Plant (KANUPP) at the coast near Karachi, which may create a cascading catastrophe similar to the 2011 Fukushima Daiichi nuclear disaster by releasing radioactive material in the ocean and atmosphere.

The historic record of cyclones and tsunamis along the coast is perplexing due to the scarcity of historical records and the paleo-dynamics of extreme wave events, which impedes hazard assessment. Further, the study area lacks field investigations for the paleo-extreme wave events to approximate their recurrence intervals and coastal impacts. Significant exploratory work has been carried out along Oman's neighbouring coastlines (Donato et al., 2008, 2009; Pilarczyk et al., 2011; Hoffmann et al., 2013, 2013a,b, 2014, 2015, 2020; Hoffmann and Reicherter, 2014; Koster et al., 2014), Iran (Shah-Hosseini et al., 2011; Yassini et al., 2016) and India ([illegible], 2013; Bhatt et al., 2016; Gandhi et al., 2017; Prizomwala et al., 2015, 2018, 2020, 2022), where sedimentary deposits (tsunamites) from extreme wave events are reported. These pieces of evidence suggest that the northern Arabian coastline was repeatedly hit by extreme waves. These extreme events are mostly attributed to the tectonic and climatic settings of the region.

* Corresponding author at: Institute of Neotectonics and Natural Hazards, RWTH Aachen University, Lochnerstr. 4-20, 52056 Aachen, Germany.
E-mail address: haider@nug.rwth-aachen.de (R. Haider).

https://doi.org/10.1016/j.margeo.2023.107032
Received 8 December 2022; Received in revised form 3 March 2023; Accepted 20 March 2023
Available online 24 March 2023

From a tectonic perspective, the Makran Coast is highly susceptible to tsunamis and the Makran Subduction Zone (MSZ) is the main source of tsunamigenic earthquakes. Since 1945, the Coast has witnessed two tsunamigenic earthquakes; a major one in 1945 (Mw 8.1) claiming some hundred human lives (Pendse, 1946; Heidarzadeh et al., 2008a, 2008b) and a minor tsunami in 2013 (Mw 7.7) with no losses (Heidarzadeh and Satake, 2014a).

So far, at the Makran Coast, either a deterministic or probabilistic approach is used to assess the tsunami hazard. The probabilistic approach is considered mature (Rashid et al., 2021) due to the advantage of equating the contribution of possible small and large events and of treating different sources of uncertainty (El-Hussain et al., 2018). On the other hand, the deterministic approach considers a specific scenario that involves various components, including (i) source type and its parameterization, (ii) modelling tsunami generation and its propagation in shallow and deep ocean; and (iii) simulation of coastal inundation (Heidarzadeh et al., 2008b). For coastal engineering, a deterministic approach is considered more useful as it allows the determination of the worst-case scenario (max. Wave height, inundation extent and depth) to design an engineering structure and also avoids the complications associated with probabilistic analysis. For near-field tsunamis, the problems with these approaches are associated with large data gaps, the maximum hazard potential and its spatial distribution. Furthermore, the former approach also entails knowledge gaps, assumptions and uncertainties. Also, there is no single accepted way of defining the worst-case scenario. Multidisciplinary and multiproxy approaches improve hazard and risk assessment (Rashid et al., 2016; De Martini et al., 2021; Rashid et al., 2013, 2016, 2018). Regarding integrated analysis, the Makran Coast probabilistic and deterministic approaches are integrated for hazard and risk assessment by (Khan et al., 2020a, 2020b; Schneider et al., 2023; Rashid et al., 2020; Yang et al., 2022). Here, we compiled and integrated five different approaches (geophysical, sedimentological-geomorphic, probabilistic modelling, numerical modelling and historical record), which we called a synergic approach for hazard assessment. As each approach has its own limitations, the synergic analysis provides better outcomes and a higher level of confidence. A key tool for coastal risk assessment is the use of inundation maps. Few studies on inundation analysis have been conducted so. Heidarzadeh et al. (2008a, 2009b) created inundation models for the cities of Pasni and Karachi using 100 m topographic resolution and 12 m wave height. Mahmood et al. (2012) modelled Gwadar for a 5.7 m high wave on the 90 m topography of the Shuttle Radar Topography Mission (SRTM). Surface topography with a resolution of at least 25 m is considered suitable for inundation analysis and evacuation planning (Griffin et al., 2015). The resolution of topography used in both cases is too coarse for risk assessment. In this study, 12 m topography is used for inundation analysis with four different wave heights (5, 7, 10, 15 m) for the cities of Karachi, Gwadar, Pasni and Ormara. The outcomes are presented as maps delineating the areas at risk. The objective of the paper is to assess the maximum tsunami hazard potential at the Makran Coast through a multiproxy approach as discussed above. Further, based on the hazard potential, areas vulnerable to extreme events are demarcated in four major cities.

2. Study area

2.1. Geodynamics

The geodynamics of the study area is evolving from the interaction of three tectonic plates: the Eurasian, Indian, and Arabian plates (see

Fig. 1. Location map showing the regional plate tectonic setting (red) and the major cyclone tracks (grey) which hit the coasts in the Arabian Sea. The size of the grey circle on the cyclone tracks corresponds to the Saffir-Simpson Hurricane Scale. Data source: International Best Track Archive for Climate Stewardship (IBTrACS) (Knapp et al., 2010). Earthquake data: International Seismological Centre (ISC 2022). (For interpretation of the references to colour in this figure legend, the reader is referred to the web version of this article.)

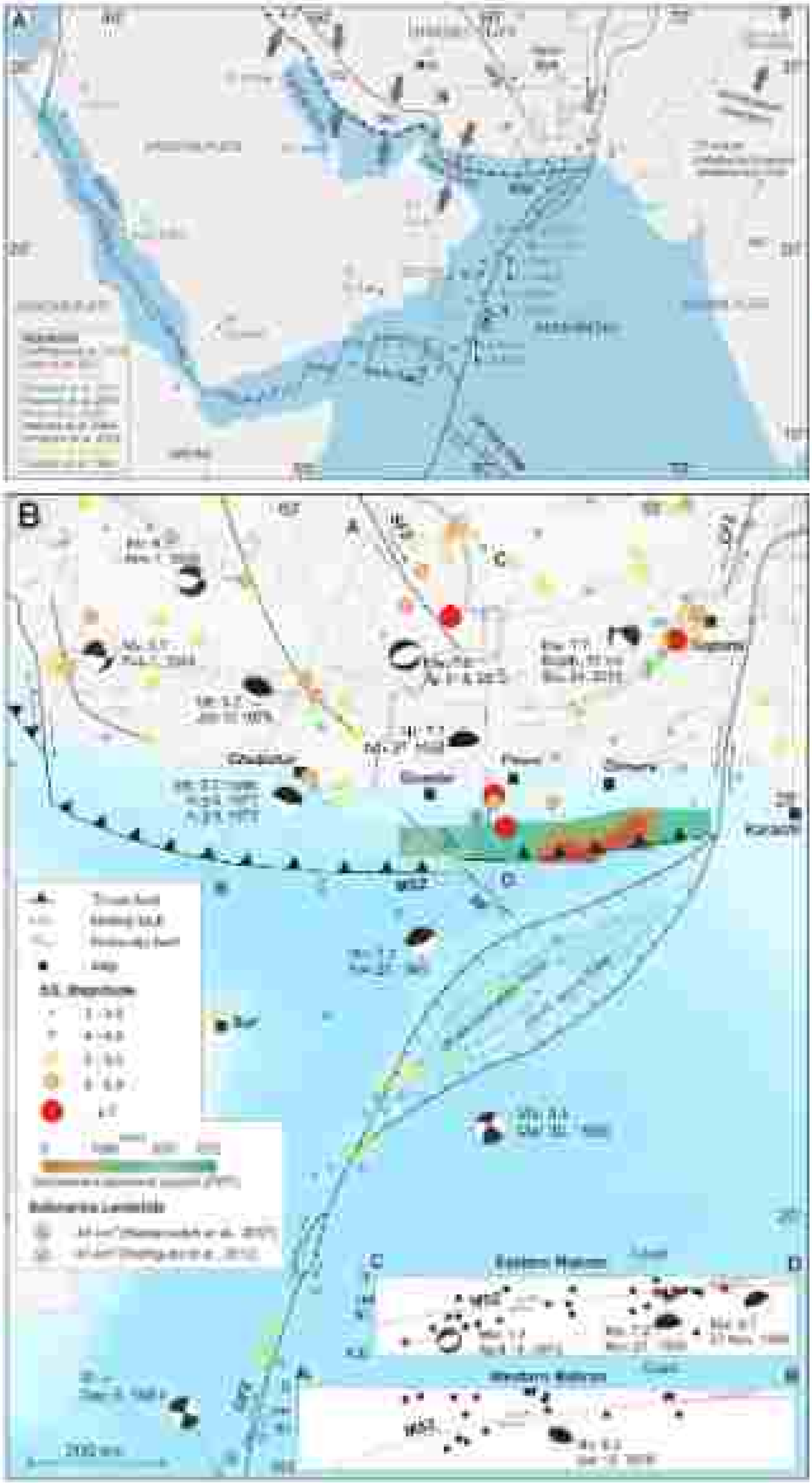

Fig. 2. A: Figure showing the tectonic setting and the geodetic motions of the study area. All the velocity vectors are in millimetres (mm). Black arrows (thin): GPS vectors; B: perpendicular vectors; N: normal vectors; grey arrows (width): convergence vectors. Different numbers against the vectors show reporting by different researchers, as indicated by different colours in the legend. Makran Subduction Zone (MSZ), Chaman-Ornach Nal Fault Zone (CFZ), Owen Fracture Zone (OFZ), Sonne Fault Zone (SFZ), Sonne Fault (SF).
B: Seismo-tectonic map of the region. Earthquake focal mechanisms are compiled from [illegible] and [illegible] (1996); [illegible] and [illegible] (1983); [illegible] et al. (2005); [illegible] et al. (2021). The simplified two-way travel time (TWT) map is from [illegible] et al. (2022) showing the nature of the contact between the accretionary and basement. The cross-sections are (adapted) from [illegible] et al. ([illegible]).

Fig. 2). The Eurasian plate is further segmented into minor plates, known as "blocks." Similarly, the Arabian Plate also has a subsurface microplate known as the Ormara plate (Kukowski et al., 2000). The tectonic accommodation between these plates is complex and depends on the crust type at the converging fronts, the relative speed and the direction of plate motion. Plate interactions are variable, but along some boundaries certain patterns can be observed (see Fig. 2A).

The rate of spreading at the mid-oceanic ridge (Red Sea) gradually increases from 7.1 ± 0.2 mm at the north to 23.55 ± 0.2 mm to the south at Sheba Ridge (ArRajehi et al., 2010). This pattern of divergence is likewise accommodated at the Makran and Zagros subduction, zones with average dipping of 3 degrees (Kopp et al., 2000), 2 degrees (White and Louden, 1982). The convergence rate increases from 4 ± 2 mm in the Persian Gulf to 19 ± 2 mm in the Gulf of Oman (Vernant et al., 2004). The plate dynamics at the eastern part of the MSZ are anomalous, as the GPS velocity at the Pasni Coast is about half the speed of its eastern and western parts (Khan et al., 2008), which reflects a partial locking at the high-friction subduction zone. The Arabian Plate forms transform boundary with the Indian Plate with a relative motion of 3 ± 1 mm/y (Bellinger et al., 2004; Fournier et al., 2008; Rodriguez et al., 2011).

2.2. Seismicity

Submarine earthquakes have triggered around 80% of the total tsunami events documented globally (Harbitz et al., 2014; Løvholt, 2017). The remaining 20% are caused by landslides, volcanoes and meteoric impacts in water bodies (Rahman et al., 2021). Overall, the study area is moderately seismic, but events like the 1945 tsunamigenic earthquake (Mw 8.1) have created uncertainty. The seismicity along the MSZ is not uniformly distributed; the western part of the MSZ (offshore Iran) is relatively silent as compared with its eastern part (offshore Pakistan). The silence in the western Makran indicates either aseismic subduction or the interlocking of plate boundaries, which can generate great earthquakes with long recurrence intervals (Byrne et al., 1992). Geodetic measurements show 19.5 mm/y convergence (Vernant et al., 2004), therefore it is not locked (see Fig. 2). The Eastern MSZ is seismically active and most of this activity is attributed to the Sonne Fault (Kukowski et al., 2000). Smith et al. (2013) relates this seismicity to the nature of the décollement. The décollement on the south-west of Pasni is brittle as indicated by high seismic velocities (>4.4 km/s). The brittle behaviour is due to the absence of soft sediments (very thin or none) in contrast to its western part. The velocities of these sediments are comparable to those observed at depth in the December 2004 Sumatra rupture area. The thermal modelling of MSZ shows that it has a potential to trigger an Mw 9.2 earthquake (Smith et al., 2013). Another thermal modelling study shows its potential as Mw 8.65 ± 0.26 and 8.75 ± 0.26 in western (Iran) and eastern (Pakistan) Makran respectively (Khaledzadeh and Ghods, 2022). Regarding the 1945 tsunamigenic earthquake (Mw 8.1), Laane and Chen (1989) through P-wave first motion studies suggested that the event has a large component of normal faulting instead and proposed a lithospheric normal faulting event usually associated with down-going slabs of old age. In contrast, the detailed studies on the focal mechanism of the 1945 Makran earthquake by Byrne et al. (1992) show that it is related to a thrust event. Their dislocation models, body waveform inversion and moment consensus indicate that the earthquake ruptured 100 to 200 km of crust along the arc in a down-dip direction. The Murray Ridge has been the consistent region of small earthquakes due to right-lateral strike-slip and normal faulting (Quittmeyer and Kafka, 1984). Quittmeyer et al. (1979) confine the seismicity only along its north-eastern half. The seismicity along the OFZ is also low to moderate, the maximum magnitude recorded is Mw 5.8 earthquake (Rodriguez et al., 2011).

2.3. Submarine landslide potential

An underwater landslide has the potential to displace a large amount of water, which generates a set of waves formally known as a tsunami (Heidarzadeh and Satake, 2017; Salah et al., 2018; Løvholt et al., 2020; Salamon et al., 2022). Mostly, under normal conditions, loose submarine sediments can withstand an angle of 12°-30° (Salama and Ghazi, 2015) but other factors, especially seismic shaking can trigger a landslide with even lower steepness. The Arabian Sea has a considerable potential for the huge offshore landslides due to a 7 km-thick sedimentary sequence in the Makran Accretionary Prism (MAP) (White and Louden, 1982) and a ~ 500 m thick pelagic drape on Owen Ridge (Shipboard Scientific Party, 1989). The high erosion rate is interpreted for these thick sequences (Kukowski et al., 2001; Ellouz et al., 2007).

The tsunamis of 1945 and 2013 are the most recent examples from the study area, which have been hypothesized to have been generated by offshore landslides (Heidarzadeh and Satake, 2014a, 2014b; Hoffmann et al., 2014). In the 1945 tsunami, there was a 2 h delay between the earthquake and the first tsunami wave at Pasni, situated at about 40 km from the epicenter (Pendse, 1948). To explain this delay, Rastgoftar et al. (2019) through inverse numerical modelling argued for a 2 h delay due to multi-wave reflection and amplification phenomena. Heidarzadeh and Satake (2017) simulated three possible secondary sources (splay faulting, delayed ruptures, and submarine landslides) and proposed that only a submarine landslide having a volume of ~40 km3 (see Fig. 2B) can reproduce the nearfield tsunami of 1945 at Pasni and Karachi.

On the bathymetric map of MAP, Kukowski et al. (2001) and Ellouz et al. (2007) identified many circular and linear slump scars. Grando and McClay (2007) interpreted slumping phenomena on the seismic lines. Slumping on MAP is generally noticed on the frontal, south-dipping folded limb, where the thrust faults propagated by folds have achieved significant height and relief. Mouchot et al. (2010) suggested that in this active setting, slope instabilities seem frequent but limited in size. Fisk et al. (2022) attributes the slumping and the very rough morphology of the upper slope to the active uplift and actual erosion. The mass movements ultimately settle in the deeper parts as turbidites. The age of the Late Quaternary turbidite sequence (sedimentary cores) and earthquake record show a good correlation (Prins et al., 2000; Bourget et al., 2011).

Along the Owen Ridge, Fournier et al. (2011) and Rodriguez et al. (2012, 2013) mapped the several types of giant mass failures along the western side of Owen Ridge by using the multibeam bathymetry and sediment echo-sounder. Southern Owen Ridge displays the largest failure area and the most voluminous landslides and the highest estimated volume of evacuated material during a landslide is up to 45 km3 (see Fig. 2B). Their research shows that the mass-wasting frequency is low due to the climatic nature and slow sedimentation rate, but earthquakes are more frequent, implying that mass failures are severely limited by sedimentation rates. In the eastern most part, the landslide potential of the Indus Delta is the least studied. The Indus River (prior to modern damming) used to supply at least 250 Mt./year to the Arabian Sea (Milliman and Syvitski, 1992), other estimates emphasize a larger range of 100 to 675 Mt./year (Ali and De Boer, 2008). Since the last glaciation, the Indus River has shed about 4050–5678 km3 of sediment into the Arabian Sea and about half of the stored sediments lie offshore on the shelf and in the submarine Indus canyon (Clift and Giosan, 2014). The massive accumulation of sediments in the offshore and canyon areas makes the delta vulnerable to landslides and necessitates further investigation.

2.4. Cyclones

In the Arabian Sea, tropical storms, also called cyclones, mostly develop either before the monsoon (May–June) or after the monsoon (October–November) with an almost equal ratio. Cyclones form when the temperature of the surface water rises above 25 °C, preferably between 28 and 29 °C (V. K. Singh and Roxy, 2022). The rising temperature develops a low-pressure region (961 hPa in the 1998 Gujarat Cyclone), which shifts laterally. The cyclones preferentially develop over the south-eastern quadrant of the Arabian Sea and sometimes a few of those develop in the Bay of Bengal and in their course of landfall, they gradually turn into depressions or well-marked low-pressure areas, but as they approach the Arabian Sea, they intensify into new cyclones. The cyclones Shaheen 2021 and Yemyin 2007 in the Arabian Sea developed from the remnants of Gulab Cyclone and Deep Depression BOB 03/2007, respectively, in the Bay of Bengal. In the Arabian Sea, the Coriolis force sometimes recurves the cyclone track clockwise towards the north-western coast of India and Pakistan (Pusphan, 2007).

3. Methodology and data

Multidisciplinary and multiproxy approaches improve hazard and risk assessment (Kawamura et al., 2014; De Martini et al., 2021; Kääb et al., 2015; Kääb et al., 2013, 2019, 2018). At the Makran Coast, PTHA and DTHA are used together by (Khan et al., 2022a, 2022b; El-Hussain et al., 2018; Salamanca et al., 2016; Yang et al., 2022; Zafarani et al., 2022). We compiled and integrated five different approaches (geophysical, PTHA, DTHA, sedimentary tsunami deposits, and historical record), which we called a synergic approach for hazard and risk assessment. The data and workflow are summarized in Table 1 and Fig. 3, respectively. The problems with PTHA and DTHA are associated with large data gaps, maximum hazard potential determination, spatial distribution, assumed and uncertain variables and different computational types (Thompson, 2005; Behrens et al., 2021). To improve hazard assessment, the PTHA (see Fig. 3) and DTHA (see Table 2) results are compared with the more meticulously evaluated seismic hazard potential (PGA), which includes weightings from the area's tectonic elements and occurrence intervals. Further, analysis of the occurrence interval is improved by the compilation and correlation of historical records (see Table 3 in the supplemental) and tsunamites records discovered at different sites around the Arabian Sea (see Table 3). For these tsunami deposits, MSZ is inferred as the tsunami source except for one mentioned in the table.

To assess the maximum wave potential, the tsunamites record of 1000 CE is taken as the worst-case discovered so far. This worst-case attribution is due to its high frequency in Table 3 and its far-flung spatial distribution (eastern and south-eastern Indian and Omani Coasts), which reflects that the event was not local but regional and of a high scale. The tsunami boulder deposits at Fins-Sur, Oman, are up to 40 tons for which an approximate wave velocity of 4.5–6.6 m/s is calculated for dislodging, uplift and transport (Hoffmann et al., 2013a, 2013b) with maximum run-up height of >17 m (Hoffmann et al., 2014). The numerical inundation modelling of wave velocities for Mw 9.0 is between 7 and 11 m/s by Mohammed et al. (2015). The deterministic rig models for Mw 9.0 earthquake, TSUNAMI-N2, MOST 21.EM, COMCOT by Heidarzadeh et al. (2008a, 2009b), Payande et al. (2015), Rashidi et al. (2018a, 2018b) can produce a maximum amplitude of 15 m, 18 m and 25 m respectively. Two studies on the thermal modelling of decollement, Mw 9.2 and Mw 8.7 by Smith et al. (2013) and Khaledzadeh and Ghods, (2022) respectively suggest the Mw 9.0 earthquake mechanism hypothesis. The probabilistic models are finally considered; the tsunami probability of ≥12 m is 0.8 in 5000 years (Heidarzadeh et al., 2009) but as of Salamon et al. (2022) it is 0.8 in 2475 years. The probable PGA value of 1.3 with a return period of 2500 years capable of generating a Mw 8.3 earthquake (Ahmed et al., 2018; Waseem et al., 2019, 2020) is in close agreement with the Zafarani et al. (2022) model. The results of Khan et al. (2022a, 2022b) are entirely different as they calculated the occurrence interval for this much intensity as 75 years, as the well-known historical record of the last 250 years does not account for such an interval.

The second part of the study includes a preliminary inundation analysis based on the evaluated hazard index. For inundation studies, cyclones are another source to be considered. The cyclone hazard map of the Arabian Sea is produced through interpolation of the historical cyclone record since 1842. The data is available from the International Best Track Archive for Climate Stewardship (IBTrACS), 2022. The entire region is classified into five hazard indices based on track density using natural neighbour interpolation. The cyclones are categorized according to the Saffir-Simpson Scale, which is based on the central pressure and the wind speed. A research gap exists in storm surge modelling along the Makran Coast. Moreover, the wavelength of tsunamis is much larger and more devastating as compared with storm surges. For crude estimation, the maximum storm surge heights of some historic cyclones in the Arabian Sea are compiled in Table 4 (supplemental).

Using the bathtub approach, flow depths are computed by inundation height and local topography difference. The method assumes a maximum uniform wave run-up consistent with tsunamites recorded along the shoreline and floods the base level connected to the beach. The approach, in sometimes modified versions, is used to study the tsunami risk assessments in Tohoku, Japan (Okumura et al., 2017); Alexb, Greece (Tselentis et al., 2011); Samoa, Pacific (Grant et al., 2018); Muscat, Oman (Schneider et al., 2016); Augusta, Italy (Pagnoni et al., 2021; Williams et al., 2021). The static bathtub approach is modified in our

Table 1
Approaches, methodologies and data used.

	Approach	Methodology/Model	Data/References
Cyclonic hazard	Probabilistic	Map based on cyclone density tracks	IBTrACS, (1842–2022)
Seismic hazard	Probabilistic	Poissonian model, (Cornell and Vanmarcke, 1969)	Khan et al. (2022a, 2022b)
		Cornell–McGuire (1968, 1976)	Waseem et al. (2019, 2020)
		UBC 97 (International Conference of Building Officials 1997)	Ahmed et al. (2018)
	Deterministic	Ambraseys and Bommer (1991) Model	Khan et al. (2022a, 2022b)
	Probabilistic	Synthetic tsunami EQ catalogue spanning over 5 million years	Heidarzadeh et al. (2009)
		Logic tree technique	Zafarani et al. (2022)
Tsunami hazard	Deterministic	Tsunami triggered by faults and landslide-based parameters	Compiled 30 deterministic tsunami models (Table 2)
	Historical Tsunami	Makran historical and instrumental great earthquakes with Mw > 8.0	Updated after Heidarzadeh et al. (2008)
	Tsunamites Record	Compilation of tsunamites discovered at different coasts along the Arabian Sea	Compiled 14 onshore & offshore tsunamites
Risk assessment	Bathtub approach	Tohoku, Japan (Okumura et al., 2017) Alexb, Greece (Tselentis et al., 2011) Samoa, Pacific (Grant et al., 2018) Muscat, Oman (Schneider et al., 2016) Augusta, Italy (Pagnoni et al., 2021; Williams et al., 2021)	DEM: TanDEM-X 0.4 arcsec (12 m) Land use: Google Earth-ESRI imagery, Open Street Maps (OSM), and the city survey & planning maps Statistics Bureau of Pakistan, 2017

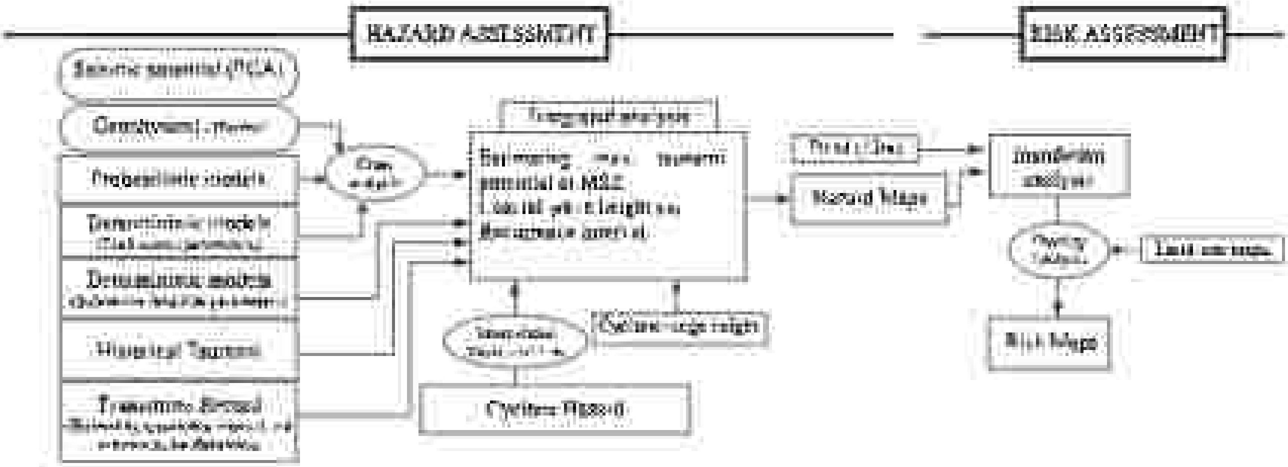

Fig. 3. Flowchart showing sequential order of various processes used for hazard and risk assessment.

ways for this study: 1) the tsunamites record the highest inundation heights as reported from the Sur/Fins coast, Oman, which is at nearly equal distance to south of the Makran Coast. The tsunami mechanism for both of these coasts is inferred to be the same as the MSZ. Further, these runup heights are compared with the probabilistic and deterministic models and finally four different wave heights (5, 7, 10, 15 m) for four major cities (Karachi, Gwadar, Ormara and Pasni). These wave scenarios under 15 m are also analysed for a possible shorter return period. For inundation analysis, the German Aerospace Centre's TanDEM-X 0.4 arcsec digital elevation model (DEM) with a spatial resolution of 12 m is used (see Fig. 4). The TanDEM-X in combination with TerraSAR-X generates DEM from bistatic X-Band interferometric SAR acquisitions. A true or bare ground elevation model or digital terrain model (DTM) is important for setting up the base level for the inundating sea water. The DEM is converted into the DTM by subtracting the approximate heights of the features like plants, houses and poles. The interpolation of open or bare land elevations to buildings, plants, and poles produced the best results for DTM conversion (see Fig. 4). All the processing and analysis are performed in GIS environment using ArcMap 10.8.

The bathtub approach's static nature has the disadvantage of inaccuracy in the estimation of flux, levelling, and gently rising terrain (Kasprzak, 2012), which have been addressed globally in several publications through hydro-morphodynamic numerical modelling especially in the Indian Ocean tsunami 2004 (Kuswanto et al., 2011), western Greece (Röbke et al., 2013, Röbke et al., 2016, 2018, 2019), Tohoku, Japan tsunami 2011 (Kuribayashi et al., 2014), Hilo Bay, Hawaii-Chilean Tsunami 1960 (Liu et al., 1995), German Bight, Germany (Oumeraci-Bouramdane et al., 2015).

4. Results

The results from the multi-proxy approach imply that the MSZ has the potential to trigger M_w 9.0 tsunamigenic earthquake with a recurrence interval between 500 and 1000 years, which may generate a tsunami up to 17.3 m (see Fig. 5 and Table 2). The region south of Pasni is more susceptible to tsunamis due to high seismic activity. In this area, the rigid decollement (Smith et al., 2013), relative geodetic plate motions at Pasni (see Fig. 2) and differential motion(s) between the Sonne fault and MSZ (Kukowski et al., 2000) indicate stress accumulation and release in the area. In this regard, further investigations and evaluations are highly recommended. The seismic and tsunami hazards are very low for a 50-year recurrence interval. The historical record of tsunamis is insufficient and data credibility may be another issue for result validation; however, a compilation of tsunamites bordering the Arabian Sea shows that these events occur every 500 years. For hazard assessment, the estimation of underwater landslides is yet another important milestone to cover, and it has serious implications on the recurrence interval.

The analysis of the cyclonic record since 1958 shows that the intensity and frequency of Category ≥1 cyclones have increased at an alarming rate (see Fig. 6B). In the last 64 years, the trend trajectory of intensity has raised three intensity levels, from tropical storm (TS) to Category-3. Since 1963, 27 cyclones have been reported, and of these, 14 have developed in the last 7 years. The frequency has increased from 1 cyclone per 10 years from 1963 to 93 to 4 cyclones per 10 years in the following 20 years (1994–2014). The situation has deteriorated further, with two cyclones per year recorded in the last seven years (2015–2021).

The cyclone track density is highest in a linear manner trending north-south at about 250 km in the Arabian Sea west of the Indian Peninsula (see Fig. 6A, B). At this linear patch, the sea surface temperature of ≥27 °C (V. K. Singh and Roxy, 2022) affects the general wind circulation and reduces the vertical wind shear, which aids the development of tropical cyclones (Gray, 1968; Murty, 1984; Zhang and Wilson, 2019, Singh et al., 2020; Sun et al., 2021). Fig. 6B shows three major routes from the main cyclone centre; first leading to Yemen-Oman border and second to cities of Hilf and Muscat and third one leads to India-Pakistan Border region (see Fig. 6B). At times, the cyclones enter the Arabian Sea from the Bay of Bengal and get amplified due to local climatic conditions in the Arabian Sea, as happened in 2007 and 2021. The sea surface temperature of the Arabian Sea has increased by 1.2–1.4 °C in the last four decades, and this rapid rise is attributed to global warming (V. K. Singh and Roxy, 2022). These ocean warmings may continue in the future, and they need to be closely monitored for the cyclone forecast models (Chandler and Lee, 2006; Singh et al., 2020). Most of the population in Gwadar, Pasni, and Ormara lives between 2 and 7 m above sea level and within 1 km of the coast. In these three cities, there are around 0.15 million people. According to rough estimates, 8 million people live between 2 and 15 m above sea level in Karachi. The inundation results for each city are explained separately as follows:

4.1. Gwadar

Gwadar city will bear no damage from the waves as high as 5 m (see Fig. 7). It can only cause minor damage to the ships and boats anchored in the eastern and western bays. The embankments are 4 m from the high tide limit, which would not allow the waves to spill over the population. Waves with a 7 m amplitude have the considerable potential to invade the city. These waves can cause moderate damage to infrastructure and claim human lives. The houses with low BVI will bear severe damage and a 10 m wave scenario will cause serious damage to

Table 2

A- The compilation of various tsunamis with fault source parameters in [illegible] and adjacent [illegible]. B- The compilation of various tsunamis [illegible] source parameters in Arabian Sea.

	Long.	Lat.	Magnitude (Mw)	Azimuth	Length (km)	Width (km)	Water Depth (km)	Epicenter Depth (km)	Moment (N.m)	Min Slip (m)	Max Slip (m)	Avg. Slip (m)	Dip	Rake	[illegible]	Wave Height (m)	Software/Code
[illegible] et al., 2008	24.77	58.8	7.8	270	47	25		13	2.708 × 10^18	0.8	1.8	1.28	7	90	[illegible]		[illegible]
El-Hussain et al., 2016	24.88	60.6	8.8	260	460	110						11	7	90		2	COMCOT
	24.88	64.38	8.1	265	280	70						8.8	7	90		2	
[illegible] et al., 2016	1945		8	248	38	70		27				10	7	88		1	[illegible]
	1945 EQ epicenter		8.4	248	38	70		27				10	7	88		2	[illegible]
[illegible] and [illegible], 2018	62.46	25.15	8.3	248	280	70		20				7	7	90		2	TELTASUNC
	65.75	25.23	8	290	360	168		30				11	7	90		4	
[illegible] et al., 2008	[illegible]		8.8	263	333	120		38	1.88 × 10^22			18	7	90		8-8	TELTASUNC
	[illegible]		9	263	333	180		38	1.21 × 10^22			22	7	90		12-18	
[illegible] et al., 2008a, 2008b	24.38	63.17	8.1	248	120-180	60-80	3300	27	1.8 × 10^21	0.8	8.8		7	88	17.8	13±7	TELTASUNC, TELTASUNC
[illegible] et al., 2008	25.38	64.33	8.4	240	200	130	50	20	1.8 × 10^21			7.8	8	88	2		TUNAMI-N2,
[illegible] et al., 2007			8	248	Equation Rupture = 0.80			20		Wells and Coppersmith (1994) [illegible] Equation Rupture = 1.127				88		2	
[illegible] and [illegible], 2014a				230-260	120-227	40-100		17-20	8 × 10^21 [illegible]			8-11	5-9	75-112		8-8	TUNAMI
[illegible] et al., 2008	1945 EQ epicenter		8.1	248	183	73		13				7	7	80		2	TUNAMI-N2,
[illegible] and [illegible], 2008	[illegible]			283									7	80		2	[illegible]
	[illegible]			280-283	[illegible]								7	80		~2	
[illegible] et al., 2008	24.88	63.60	8.8	270	200	200	5000	30				18	10	90		7	[illegible]
[illegible] et al., 2008	25	24	8.1	248	45-120	83		13				8-20	7	80		2-14	
[illegible] and [illegible], 2010	1945 EQ epicenter		8.8									3.38				2	[illegible]
[illegible] et al., 2011	1945 EQ epicenter		8	380	387	190		38				11	7	90		3 to 8	TELTASUNC
[illegible] et al., 2011	EQ-1945 [illegible]		8.1	270	220	120		30				18	12	90		3 to 5	TELTASUNC
[illegible] et al., 2011	[illegible]		8.1	280	100-300	80		30					7	68-90		3 to 12	[illegible]
[illegible] and [illegible], 2014	61.18	24.88	9	278	280	200		30				11	7	90		8	TUNAMI-N2
	58.3	25.30	8	230	305	158		30				12	7	90		4	
	62.48	25.15	8.1	248	180	73		27				7	7	80		2.8	
[illegible] et al., 2014	1945 EQ epicenter		8.1					28									
	63.5	24.8	7.5					13								4-8	[illegible]
			8.2					28								8	
			9.1					30								28	
[illegible] et al., 2014	[illegible]		8.8	288	284	130						8	15	80		1 to 4	[illegible]
	[illegible]		7.7	288	108	43						2	30	90		1 to 3.3	
	[illegible]		7.8	48	137	43						2.2	88	180		1 to 2.2	

(continued on next page)

Table 2 (continued)

	Long.	Lat.	Magnitude (Mw)	Azimuth	Length (km)	Width (km)	Water Depth (m)	Epicenter Depth (km)	Moment (N m)	Min Slip (m)	Max Slip (m)	Avg. Slip (m)	Dip	Rake	Top (km)	Wave Height (m)	Software/Code
[illegible] et al., 2013	63.20	24.73	7–8.3	270	100–150	30		7.00				0.05–0.83	3	90		Max 1.8	ComMIT
[illegible] et al., 2016	1883		8.2		300	150						15				15	TUNAMI
			8.8		550	225						15				15	
			8.2		55	80						8.2				8	
			8.2		55	75						4.2–13				8	
[illegible] et al., 2017	1945 EQ epicenter		8.1	248	180	70	3000	27	1.8 x 10^{21}			6.6	7	89	2	5	ComMIT
			8.1	270	180	70			1.8 x 10^{21}			15		90		15	
[illegible] et al., 2018a	Iranian Makran		9	280	400	150		33	1.05 x 10^{22}			23	7	90		10	COMCOT
			7.7	280	208	40	3000			3			23	90		2	
			7.8	45	187	48	3000			3.5			88			2	
[illegible] et al., 2018a, 2018b			8					33	4.5 x 10^{22}					88		23	

B	Longitude	Latitude	Bulk Density (kg m^3)	Viscosity (m^2/s)	Initial Submergence (Travel Distance) (m)	Water Depth (m)	Seabed Slope (degree)	Volume (km^3)	Slide Length (km)	Slide Thickness (m)	Slide width (km)	Wave Height (m)	Software/ Code
[illegible] et al., 2013	63.3°	17.3		25 to 300		3000		40		140		3.3	AVALANCHE
[illegible] and [illegible], 2018	64.1	24.73			1124		6		13	400	10	Max 18–20	TOPICS and FUNWAVE
[illegible] et al., 2019	Pakistan QAT					Coastal landslides		1	22	2	10	<1	TUNAMI
								0.5	13	2	10	<1	
[illegible] and [illegible], 2019a, 2019b, 2020	63	24.8	2200		3000–3000	1200–3000		40		300		25.9	TUNAMI-N2
			2150		1000–2000	1200–3000			28	600	25	18.3	
			2050		1000–2000	1200–3000			28	600	25	13.7	
[illegible] et al., 2020	67.08	25.1	2000		300–3000	150–450				100–300	5–10.5	Max 2	JAGURS
[illegible] et al., 2020	61.3	24.4					5					0.2	
[illegible], 2020	58.75	23.87					25	4	4.5	300	4	24	COMCOT

Table 2
The compilation of tsunamites discovered at different coasts along the Arabian Sea (arrived age-wise).

Sr.	Event Year (radiometric)	Event assigned	Location	Brief detail	Reference
1	[illegible]	1945	[illegible], India	The documentary tsunamites in the [illegible] show physical, geochemical and biological characteristics such as fossil content, sharp contact with the underlying unit and lack of sorting along with the presence of mud clasts. The sedimentary layer also shows an abnormal inland extent of ~ [illegible] m from the present high-water line.	[illegible] et al., 2022
2	1945[a] Tsunamigenic earthquake event	1945		[illegible]	[illegible]
3	Older than 1945[b]	1945–	Sur Lagoon, Oman	[illegible]	[illegible] et al., [illegible]
4	[illegible]	[illegible]		[illegible]	[illegible] et al., [illegible]
6	[illegible]	[illegible]	[illegible], India	[illegible]	[illegible] et al., [illegible]
7	[illegible]	[illegible]	[illegible], Oman	[illegible]	[illegible] et al., [illegible]
8	[illegible]	[illegible]	[illegible], India	[illegible]	[illegible] et al., [illegible]
9	[illegible]	[illegible]	[illegible], India	[illegible]	[illegible] et al., [illegible]
10	4500 ± 200 BP	4500	Ras al Hadd, Oman	[illegible]	Hoffmann et al., [illegible]
11	[illegible]	[illegible]	Sur, Oman	[illegible]	[illegible] et al., [illegible]
12			[illegible], Iran	[illegible]	[illegible] et al., [illegible]
13			[illegible], India	[illegible]	[illegible]
14			[illegible], India		
15			[illegible], Oman	[illegible]	Hoffmann et al., [illegible]

[a] [illegible]
[b] [illegible]

the city. Along with inundating the city centre, it will also inundate the area planned for future industry (see Fig. 7). The 15.5 m scenario creates total havoc in the city as the tombolo neck will completely submerge under the water. According to interviews of the 1945 tsunami survivors, [illegible] towns were inundated by the 1945 Tsunami. So, it can be inferred that waves height then were at least 14 m high at the eastern bay of Gwadar. The beach topography at Gwadar is greatly altered by the construction of embankments on both sides of the bays, which reduces the efficacy of a comparative analysis with the 1945 tsunami.

4.2. Pasni

The effect of a 2 m high wave in Pasni is almost the same as that of Gwadar, but it has the potential for minor damage to the infrastructure along the beach (see Fig. 8 in the supplement). The waves up to 7 m height will have serious consequences on the town as about one third of the town submerges under the water (see Fig. 8 in the supplement). The submerged area also partly includes the densely populated city center. It will block the major road that links Pasni to the rest of the country. The 10 m wave height has the potential to inundate the entire city centre, including [illegible]. In this scenario, infrastructure and human life will suffer greatly. Almost the entire town will be affected in the 15-m scenario. At the city centre, single-story buildings will be approximately 7–10 m under water. The 1945 tsunami (12 m) comparative inundation analysis fits well with our results in Pasni, except there is a sand accretion of [illegible] m at the northern port area and a ~ 5 m high and 2.5 km long concrete barrier built at the southern port area. These barriers provide some coastal defence against the waves, especially those related to cyclones.

4.3. Ormara

Most of the population resides below 5 m elevation within 1 km of

Fig. 4. A comparison of the DEM (left) and a satellite image (right) of a section of Karachi. The buildings in the oval circle show the building elevations as compared with the ground elevations in the surroundings. The arrows and squares point to the low ground elevation sites (roads, open lands) in between the densely populated areas used for the DTM interpolation.

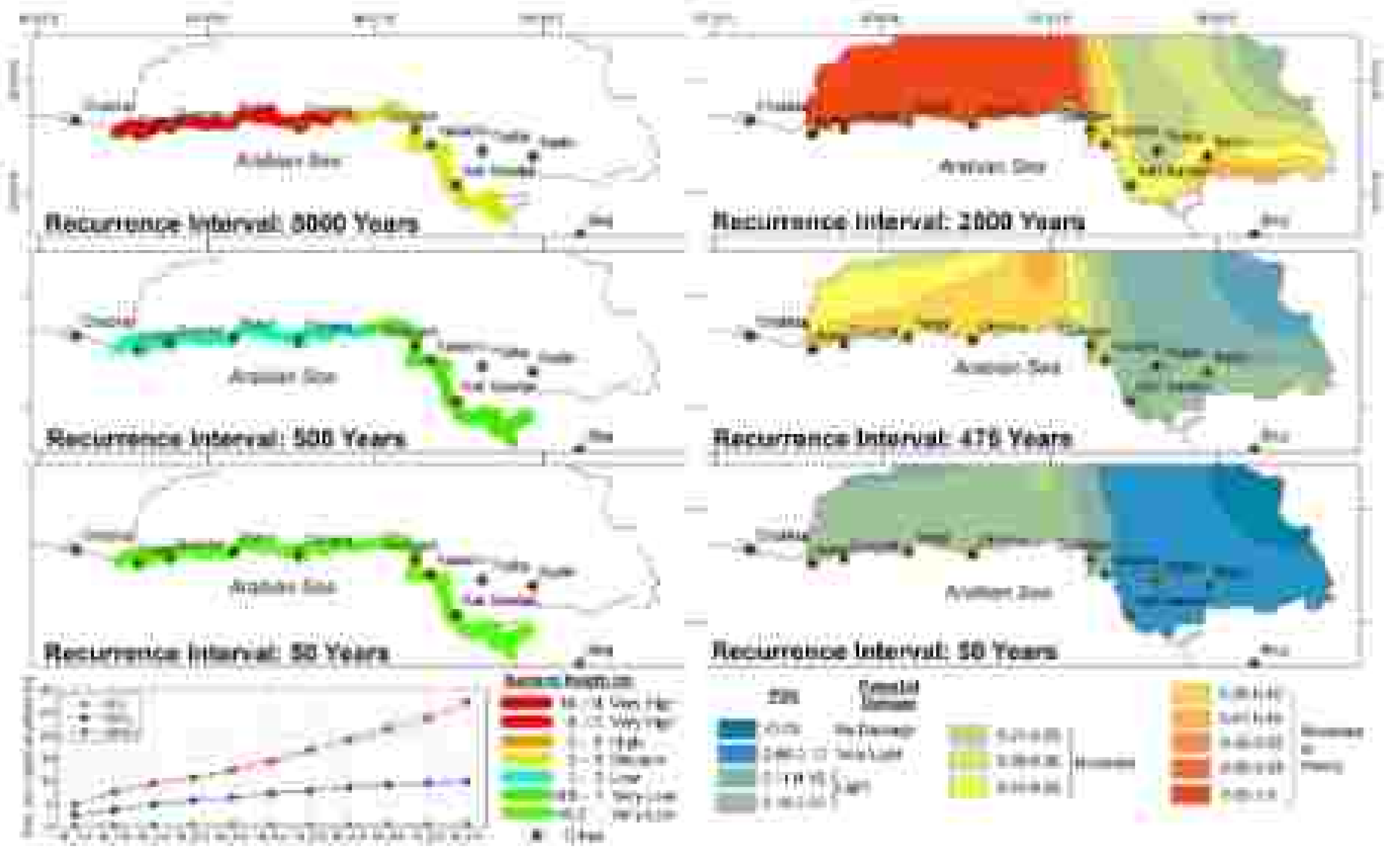

Fig. 5. The left column shows probabilistic tsunami heights with different recurrence intervals by [illegible] et al. (2018). The right column shows the seismic hazard maps based on probabilistic peak ground acceleration (PGA) for different recurrence intervals by [illegible] et al. (2018). The probability of tsunami heights is calculated from the instrumental and historical seismicity at the MSZ.

the eastern and western bays (see Fig. 9 in the supplement). In the 3 m scenario, the city undergoes minor damage to the houses along the beach, especially at the eastern bay. A 7 m tsunami wave has the potential to seriously affect the town. As estimated from the interviews of the 1945 tsunami survivors, approximately a 7 m wave affected the town. In this regard, a 10 m wave and a 15 m wave have a potential to affect the whole town with 4 m and 9 m flow depths respectively. Also, along with city, the hammer head's rock (symbolic) will completely submerge under the water.

4.4. Karachi

Karachi is the biggest city along the Makran Coast and is highly vulnerable to the extreme events. Though the evaluated hazard potential

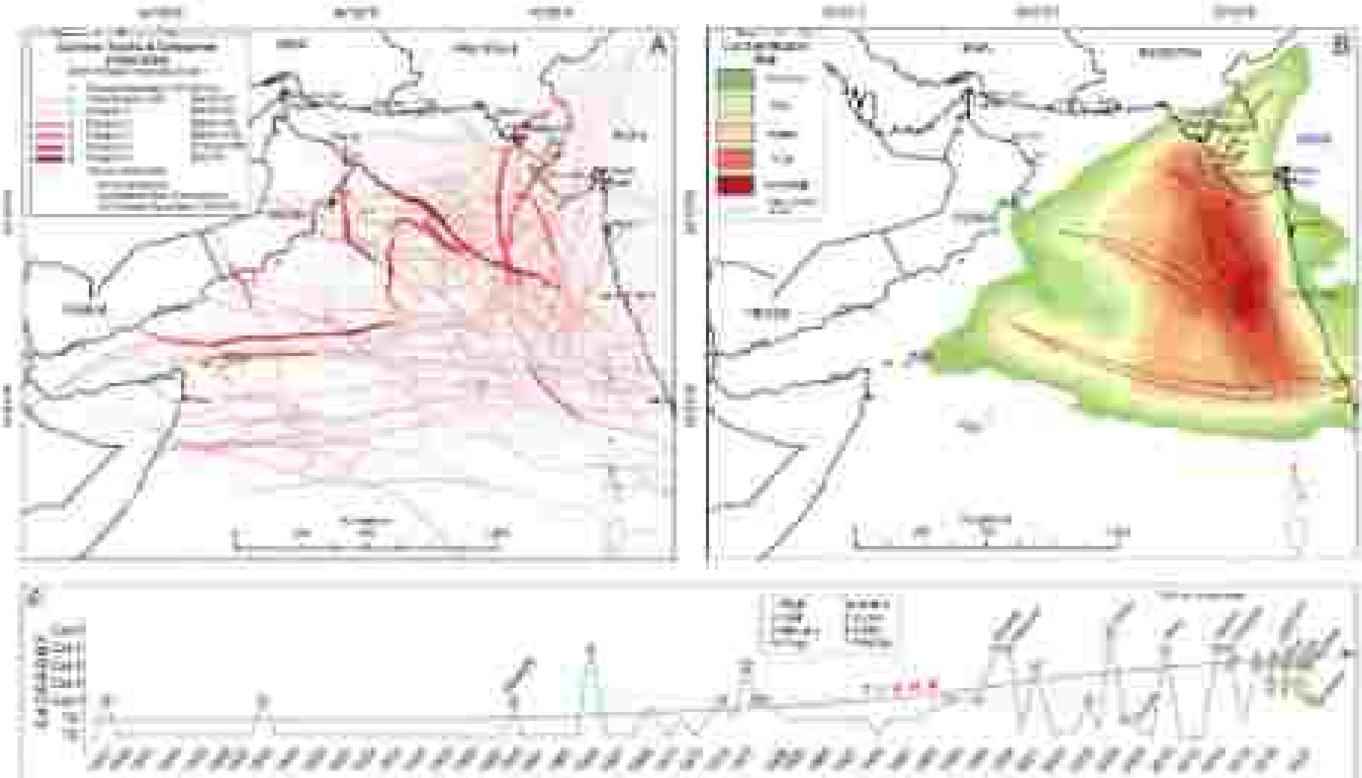

Fig. 6. A. Cyclone tracks in the Arabian Sea since 1842 (International Best Track Archive for Climate Stewardship (IBTrACS, 2020)). The segmented colour scheme shows the cyclone category. B. Cyclone hazard map based on the cyclone density. The branched structure shows the high frequency cyclone routes. C. graph shows a trend in the frequency and intensity of cyclones.

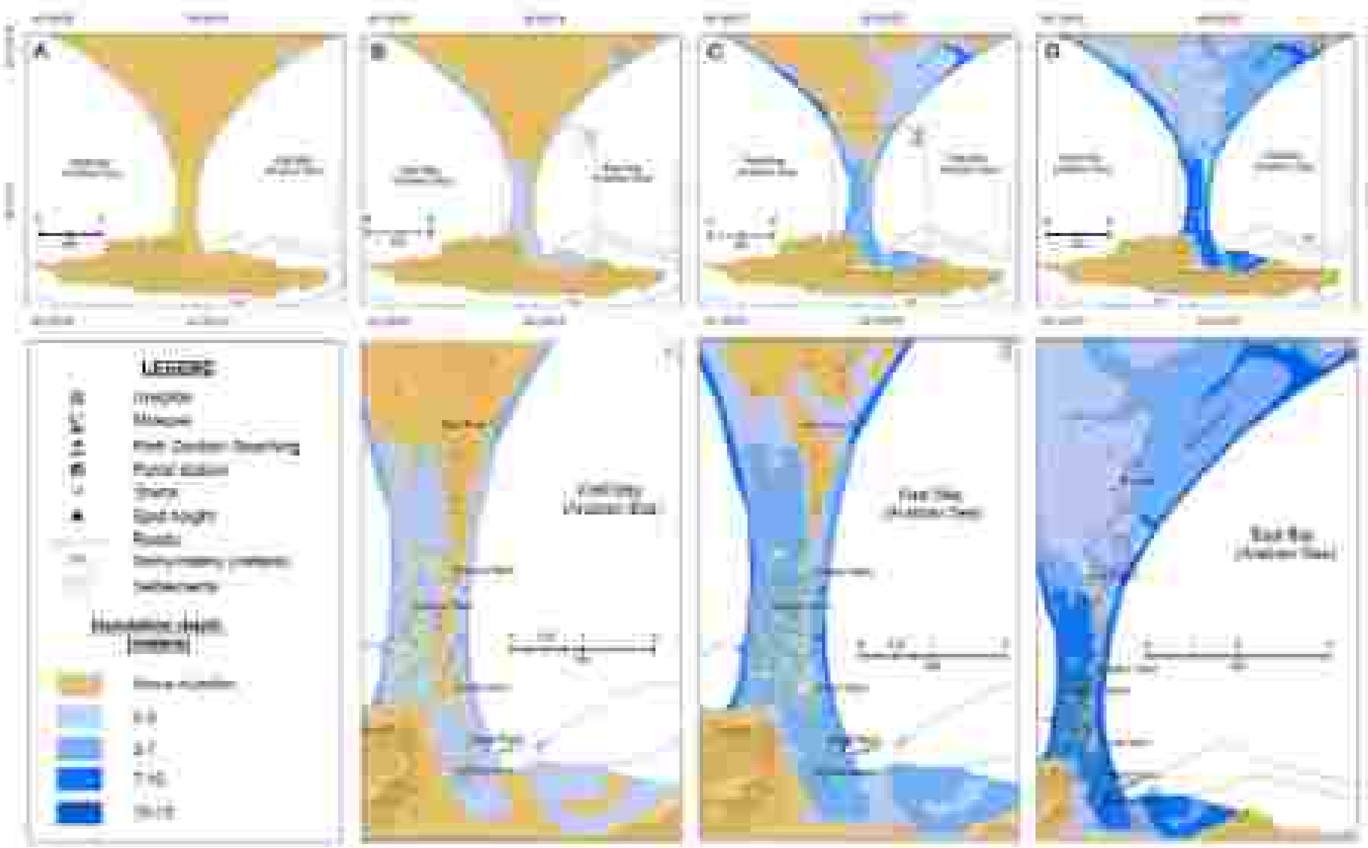

Fig. 7. Results of inundation analysis for Gwadar. A. 3 m scenario B. 7 m scenario C. 10 m scenario D. 13 m scenario.

for such extreme waves is low except for tsunamigenic landslide hazard. 5 m waves have a minor impact on Sonmiani, Clifton, the Manora-Bundal islands, and the Defence Housing Authority (DHA). The 7 m and 10 m waves will have serious consequences due to their higher tendency to inundate deep into the city (see Fig. 13 in the supplementary). Other than directly facing the shoreline, the creeks (Korangi, Gharo, Chinna) provide main pathways for a deep and far inland inundation, therefore, proximity to these creeks is at high risk (see Fig. 10). Waves of 15 m can cause significant loss of life and infrastructure damage. The Manora and Bundal islands will be submerged for >10 m in this scenario. Overcrowding, substandard buildings, proximity to the beach, and a poor economic situation increase the risk factor and reduce the society's resilience. Karachi has an advantage over the other cities in that it has many multi-storey concrete buildings, which may provide a quick vertical evacuation during such an event.

5. Discussion

The establishment of the maximum tsunami potential is essential for its hazard and risk assessment. In this regard, each approach has its own limitations, particularly gaps in knowledge, data and different computational types. As compared to a single proxy, the synergy of five proxies has improved the level of information and confidence in the hazard estimation and risk assessment. In comparative analysis for a scenario, the proxies either validate or negate and in some cases, narrow down the result range. The probability studies based on various techniques and methods estimate the recurrence interval of a mega tsunami event between 2800 and 5000 years. These probable models only take earthquake sources into account and do not consider other non-seismic tsunami sources. In this regard, considering the well-studied tsunami events of 1945 CE and 1000 CE in the northern Arabian Sea, the recurrence interval narrows down to 1000 years. With these two arguments, a quick and crude analysis implies that non-seismic tsunami sources and/or cascading sources (co-seismic landslides) generate about 40% to 50% of tsunamis in the Arabian Sea. This ratio is high, as we keep the interpretation tentative. Globally, about 80% of tsunamis have an earthquake source (Harbitz et al., 2014; Løvholt, 2017; Roberts et al., 2021). Non-seismic tsunami sources, particularly underwater landslides, complicate hazard assessment in terms of magnitude and recurrence interval. In comparison to an earthquake, a landslide has a greater potential for larger wave heights due to its large vertical slip (see Table 2S). However, the size of triggered mass characterizes the tsunami size. The 1945 (major) and 2013 (minor) tsunamis in the Arabian Sea are also attributed to a submarine landslide triggered by offshore and terrestrial earthquakes, respectively. These recent tsunami events also reflect the high frequency of underwater slope failures ([illegible] et al., 2014; Heidarzadeh and Satake, 2017). Landslide stability is dependent on several geotechnical and lithological factors (slope angle, consolidation, specific gravity, density, particle type and size, consistency limits, and compaction). Many agents can lower the threshold of these factors, especially earthquakes, submarine volcanic activity, marine life, and submarine anthropogenic activities like communication cables, mining, and drilling. Considering moderate to high-scale offshore earthquakes (Mw [illegible]) capable of destabilizing a mega submarine landslide, the frequency of slope failures should be high because these events occur every [illegible] years (Table 3 in the supplementary) and provide critical landslides that have completed or are near the completion of their angle of repose ([illegible]). The landslide-related [illegible] is an important research gap, which greatly hampers the tsunami hazard assessment. The precise measurement and monitoring of these factors to estimate their slip rates and failure times is a mammoth task.

The compilation shows the sequence of events as [illegible] B.C., 1524 CE, 1000 CE, [illegible] ± 200 BP and [illegible] ± 200 BP ([illegible]). The interval between the first three clusters of events is about 500 years, while the fourth and fifth clusters have an interval of 1500 years, but there is a gap of [illegible] years between these two clusters of events. This huge interval (3000 years) has three possible speculations. First, there was no such extreme wave event and if the event(s) occurred, either they could not be preserved in the sedimentary record or, if preserved, they have not been discovered yet. This approach has limitations: 1) Pakistan's coast lines, which are highly susceptible to tsunamigenic earthquakes and have yet to be explored for palaeotsunami deposits that could enrich ([illegible]); 2) the status of interpretation for most of them as tsunamites is tentative and not proven yet, as their deposition by other non-seismic tsunami sources and cyclones is not completely ruled out. 3) some approximation, geological inferences and assumptions, and the correlation of an extreme wave event with a previously known event, such as the 1000 CE tsunami.

For Karachi, the inundation analysis and risk results are quite complex to conclude. The complexity is due to the city's tightly packed nature and the confusing historic extreme wave record. In the tightly packed areas, SAR could not resolve the streets, roads, and land topo in some areas. The maximum wave height expected for this city is due to its location, as the high-intensity waves generated at MSZ mostly propagate in a north-south direction, and the city lies mostly to the east of MSZ. However, the deterministic models show that Karachi expects about half of the maximum wave height recorded at the Ormara. It is the easternmost city, located in a southerly direction from MSZ, and is the closest to Karachi of the three. If we apply this hypothesis to the 1945 tsunami waves, the maximum wave height calibrated and estimated at Ormara was about [illegible] m (Rashid et al., 2024). The calibration is based on claims made by 1945 tsunami survivors that Ormara city was approximately 2 m after the earthquake ([illegible]), along with interviewing senior citizens, provided solid evidence of a 2 m uplift. In Karachi, wave height was about [illegible] m as reported by the 1945 tsunami survivors (Rashid et al., 2024), but Karachi's 1945 tide gauge record shows a 32 cm waveform ([illegible]). Taking this hypothesis ahead for the Mw 9.0 (25 m slip) earthquake at MSZ, it could generate a maximum wave height of 15 m at Ormara and [illegible] m at Karachi's Coast. The nuclear power plant near Karachi is at least 15 m high from the high tide limit. Through the above discussion, we may conclude that this part of the study area is not likely to receive waves higher than 9 m. However, its vulnerability with reference to a mega-landslide needs evaluation.

The Makran Coast, due to its proximity to the MSZ could not benefit much from the far-field early warning system, namely the Indian Ocean Tsunami Warning and Mitigation System (IOTWS) installed in the Arabian Sea. With reference to a tsunami generated at MSZ, this system is beneficial for the south-western Indian Coast, including Mumbai city, as its far-field warning mechanism can work for it. Numerical modelling of 1945 tsunamigenic earthquake (Mw 8.1) shows that the tsunami reaches at Pasni, Karachi and Deep-Ocean Assessment and Reporting of Tsunami stations (DART) station in about 15, 100 and 50 min respectively ([illegible]). There is a reaction time of [illegible] min for alert issuance and evacuation. The Pakistan Meteorological Department (PMD) is the focal agency for monitoring coastal hazards and issuing warning alerts. PMD established a near-field tsunami early warning system in 2010 and a well-established cyclone early warning system is also in place. However, the tsunami reaction time (15 min) at the nearest coast is extremely short. On the resilience and preparedness side, the large number of casualties and property losses during the cyclones of 1999, 2007, 2010 and 2021 reflect a dejected level of preparedness and resilience and for tsunamis the level is even more pathetic.

6. Conclusions

This study includes a hazard and risk assessment of tsunamis and cyclones along the Makran Coast of Pakistan. The highly populated Karachi (~20 million), newly developed economic zone at Gwadar and nuclear power plant along the coast have heightened the focus of the topic. We used five approaches including probabilistic, deterministic, geophysical, sedimentary and historical analysis to estimate the wave potential in the Arabian Sea and constructed four different wave scenarios for inundation analysis. Inundation scenarios were performed in a GIS environment coupled with land use maps to demarcate the areas at high and very high risk.

Results indicate very high risk at Ormara, Pasni and Gwadar due to their orientation, low topography and proximity to the tsunami source. However, a 3 m scenario will not have a significant impact on the Gwadar due to barriers (4 m) created by newly constructed highways on both sides (see Fig. 7). Karachi is the most vulnerable city to extreme waves due to population pressure, substandard buildings, proximity to the beach, and a poor economic situation that increase the risk factor and reduce the society's resilience. However, its position with respect to the MSZ and propagating waves needs to be studied in detail. Furthermore, the nuclear power plant near Karachi is at least 15 m above the high tide line and is therefore safe, provided its other components, like the cooling systems, keep on working during the extreme wave event (see Fig. 10 in the supplement). Overall, the inundation analysis shows that the damage to the Makran Coast will be minor for 3 m, moderate for 7 m and severe for the 10–15 m and higher tsunamis, especially for the four major cities discussed in the paper. In these four cities, at least 0.7 million people are at risk. Aside from tsunami hazard, the intensity and frequency of cyclones since 1988 have increased significantly, from Tropical Storm to Category-5 with one cyclone per year respectively. The enormous number of lives and property losses during the cyclones in 1998, 1999, 2007, 2010, and 2021 reflect a disheartening level of preparedness and resilience, and the level is even more pitiful in the case of tsunamis.

6.1. Outlook

The coastline along the high tsunami hazard zone (Gwadar to Ormara) should be investigated for field evidence (tsunamites) to frame the paleo-tsunami record to estimate source potential and the recurrence interval. The active seismic zone south of Pasni in relation to the Sonmiani Fault, the nature of the decollement basement and the slow GPS velocity at Pasni should be investigated in detail. Submarine landslide potential is poorly known, but detailed bathymetric studies may help in determining the potential. Further, the high hazard zones demarcated in the studies may be revisited at regular intervals to estimate the slip rate and time of slope failure. Though the forecasting side of cyclones has greatly improved with time, the resilience and preparedness aspects are still far from satisfactory. The estuaries of Ormara and Pasni are suitable sites for mangrove forestation. The Karachi Beach (Clifton) may be turned into artificial estuaries that may serve the purpose of planting a mangrove forest. Along with many other benefits, it may act as a coastal defence structure against the extreme waves. There is a considerable scientific understanding of the earthquake and tsunami dynamics, but still there are large data and knowledge gaps, assumptions and uncertainties. Due to these shortcomings and limitations, the timing and exact location of earthquakes and tsunamis are still unpredictable (Behrens et al., 2021). Till there is a scientific breakthrough, the option in hand is to get well prepared by enhancing the community awareness and resilience.

Authors contributions

RH conceived the idea, planned the methodology, interpreted the results, and then reached conclusions. SA assisted in data interpretation and writing process. GH co-supervised the process. SK supervised the whole process and provided technical, environmental, financial, and personal support for the research work.

Financial support

The research work is generously supported by the German Academic Exchange Service (DAAD) (Research Grants-Doctoral Programmes no. 57507871).

Declaration of Competing Interest

The authors declare that they have no known competing financial interests or personal relationships that could have appeared to influence the work reported in this paper.

The authors declare the following financial interests/personal relationships which may be considered as potential competing interests:

Rashid Haider reports financial support was provided by German Academic Exchange Service (DAAD).

Data availability

All historical documents and newspaper accounts that the paper refers to can be found at https://itic.ioc-unesco.org/ (ITIC, 2021). The 12 m digital elevation model data is owned and processed by the German Aerospace Center.

Acknowledgement

We are grateful to the German Aerospace Center for providing the unprocessed digital elevation model data (TanDEM-X; DEM 12 m) for the inundation analysis.

Appendix A. Supplementary data

Supplementary data to this article can be found online at https://doi.org/10.1016/j.margeo.2023.107042.

References

Ahmad, B., Sana, H.R., Bahl, M.N., 2014. Probabilistic seismic hazard analysis based zoning map of Pakistan. J. Earthq. Eng. 1–38. https://doi.org/10.1080/13632469.2013.[illegible].

[illegible], M.R., [illegible], M., Chagh[illegible], T., [illegible], K., 2021. [illegible] tsunami waves in the gulf of Oman. J. Coast. Res. [illegible].

Ali, K.F., De Boer, D.H., 2008. Factors controlling specific sediment yield in the upper Indus River basin, northern Pakistan. Hydrol. Process. 2274, 2267–2274. https://doi.org/10.1002/hyp.[illegible].

[illegible], Y.R., Mahmood, T.S.S., Prakash, T.N., 2021. Numerical simulation of the 1945 Makran tsunami on the southwest coast and Lakshadweep islands of India. Mar. Geod. 44, 58–75. https://doi.org/10.1080/01490419.2021.[illegible].

ArRajehi, A., McClusky, S., Reilinger, R., Daoud, M., Alchalbi, A., Ergintav, S., Gomez, F., Sholan, J., Bou-Rabee, F., Ogubazghi, G., Haileab, B., Fisseha, S., Asfaw, L., Mahmoud, S., Rayan, A., Bendik, R., Kogan, L., 2010. Geodetic constraints on present-day motion of the Arabian Plate: Implications for Red Sea and Gulf of Aden rifting. Tectonics 29, 1–10. https://doi.org/10.1029/2009TC002482.

[illegible], A., [illegible], L.R., 1980. Focal mechanism of an earthquake [illegible]. Tectonophysics 79, 27–40.

Baptista, M.A., Miranda, J.M., Omira, R., El-Hussain, I., 2020. Study of the 24 September 2013 Oman Sea tsunami using linear shallow water inversion. Arab. J. Geosci. 13. https://doi.org/10.1007/s12517-020-05502-x.

Behrens, J., Løvholt, F., Jalayer, F., Lorito, S., Salgado-Gálvez, M.A., Sørensen, M., Abadie, S., Aguirre-Ayerbe, I., Aniel-Quiroga, I., Babeyko, A., Baiguera, M., Basili, R., Belliazzi, S., Grezio, A., Johnson, K., Murphy, S., Paris, R., Rafliana, I., De Risi, R., Rossetto, T., Selva, J., Taroni, M., Del Zoppo, M., Armigliato, A., Bureš, V., Cech, P., Cecioni, C., Christodoulides, P., Davies, G., Dias, F., Bayraktar, H.B., González, M., Gritsevich, M., Guillas, S., Harbitz, C.B., Kânoğlu, U., Macías, J., Papadopoulos, G.A., Polet, J., Romano, F., Salamon, A., Scala, A., Stepinac, M., Tappin, D.R., Thio, H.K., Tonini, R., Triantafyllou, I., Ulrich, T., Varini, E., Volpe, M., Vyhmeister, E., 2021. Probabilistic tsunami hazard and risk analysis: a review of research gaps. Front. Earth Sci. 9, 1–28. https://doi.org/10.3389/feart.2021.628772.

Bell, K.C., 2011. Lessons from the Reconstruction of Post-Tsunami Aceh: Build Back Better through Ensuring Women are at the Centre of Reconstruction of Land and Property. In World Bank, Washington, DC.

[illegible], E., 2015. [illegible] of Tsunami [illegible] and [illegible] in [illegible]. [illegible], p. 128.

Bhatt, N., Ukey, [illegible], Chamyal, L.S., Sivaramakrishnan, [illegible], 2016. Geological evidences of extreme waves along the Gujarat coast of western India. Nat. Hazards 84, 1685–1704. https://doi.org/10.1007/s11069-016-2507-9.

Bourget, J., Zaragosi, S., Ellouz-Zimmermann, N., Mouchot, N., Garlan, T., Schneider, J.L., Lanfumey, V., Lallemant, S., 2010. Highstand vs. lowstand turbidite system growth in the Makran active margin: Imprints of high-frequency external controls on sediment delivery mechanisms to deep water systems. Mar. Geol. 274, 187–208. https://doi.org/10.1016/j.margeo.2010.04.005.

Byrne, D.E., Sykes, L.R., Davis, D.M., 1992. Great thrust earthquakes and aseismic slip along the plate boundary of the Makran Subduction Zone. J. Geophys. Res. 97, 449–478.

[illegible], [illegible], 2014. [illegible] Tsunami [illegible] at the North Sea and [illegible] in the [illegible].

Clift, P.D., Giosan, L., 2014. Sediment fluxes and buffering in the post-glacial Indus Basin. Basin Res. 26, 369–386. https://doi.org/10.1111/bre.12038.

[illegible], 2014. Comparing the [illegible] [illegible].

[illegible], [illegible], 1998. The [illegible]. In: Proceedings of the [illegible] Conference on Earthquake Engineering, pp. [illegible].

De Martini, P.M., [illegible], 2021. The Mediterranean Sea and the Gulf of Cadiz as a natural laboratory for paleotsunami research: recent advancements. Earth-Sci. Rev. 216, 103578. https://doi.org/10.1016/j.earscirev.2021.103578.

Dhabu, V., [illegible], Hoffmann, G., 2022. Life on the Edge: A Dynamic Tsunami-Conditioned Indian Ocean Hinterland Life on the Edge: A Dynamic Tsunami-Conditioned Indian Ocean Hinterland [illegible]. https://doi.org/[illegible].

Dolatabadi, [illegible], Mohammadi, M., [illegible], 2007. Tsunami risk assessment modelling in Chabahar port, Iran. Int. Arch. Photogramm. Remote Sens. Spat. Inf. Sci. – ISPRS Arch. 42, 461–467. https://doi.org/10.5194/isprs-archives-[illegible].

Donato, S.V., Reinhardt, E.G., Boyce, J.I., Rothaus, R., Vosmer, T., 2008. Identifying tsunami deposits using bivalve shell taphonomy. Geology 36, 199–202. https://doi.org/10.1130/G24554A.1.

Donato, S.V., Reinhardt, E.G., Boyce, J.I., Pilarczyk, J.E., Jupp, B.P., 2009. Particle-size distribution of inferred tsunami deposits in Sur Lagoon, Sultanate of Oman. Mar. Geol. 257, 54–64. https://doi.org/10.1016/j.margeo.2008.10.012.

El-Hussain, I., [illegible], 2018. [illegible] and [illegible] of [illegible] tsunami deposits in northeast Oman. [illegible]. https://doi.org/[illegible].

Ellouz, N., Lallemant, S.J., Castilla, R., Mouchot, N., Leturmy, P., Battani, A., Buret, C., Chérel, L., Desaubliaux, G., Deville, E., Ferrand, J., Lügcke, A., Mahieux, G., Mascle, G., Mühr, P., Pierson-Wickmann, A.-C., Robion, P., Schmitz, J., Danish, M., Hasany, S., Shahzad, A., Tabreez, A., 2007. Offshore frontal part of the Makran accretionary prism: The Chamak Survey (Pakistan). In: Thrust Belts and Foreland Basins, Frontiers in Earth Sciences. https://doi.org/10.1007/978-3-540-69426-7_18.

Fournier, M., Patriat, P., Leroy, S., 2001. Reappraisal of the Arabia-India-Somalia triple junction kinematics. Earth Planet. Sci. Lett. 189, 103–114. https://doi.org/10.1016/S0012-821X(01)00371-5.

Fournier, M., Chamot-Rooke, N., Petit, C., Fabbri, O., Huchon, P., Maillot, B., Lepvrier, C., 2008. In situ evidence for dextral active motion at the Arabia-India plate boundary. Nat. Geosci. 1, 54–58. https://doi.org/10.1038/ngeo.2007.24.

Fournier, M., Chamot-Rooke, N., Rodriguez, M., Huchon, P., Petit, C., Beslier, M.O., Zaragosi, S., 2011. Owen Fracture Zone: The Arabia-India plate boundary unveiled. Earth Planet. Sci. Lett. 302, 247–252. https://doi.org/10.1016/j.epsl.2010.12.027.

Frank, N.L., Husain, S.A., 1971. The Deadliest Tropical Cyclone in History. Bull. Am. Meteorol. Soc. 52, 438–445. https://doi.org/10.1175/1520-0477(1971)052<0438:TDTCIH>2.0.CO;2.

Gandhi, D., Chavan, S.A., [illegible], Bhatt, N., [illegible], 2017. Testing the numerical models for boulder transport through high energy events with direct field evidence from southern Saurashtra, western India. Quat. Int. 444, 209–218. https://doi.org/10.1016/j.quaint.2016.08.005.

Gordon, R.G., Demets, C., 1989. Present-day motion along the Owen fracture zone and Dalrymple trough in the Arabian Sea. J. Geophys. Res. 94, 5560–5570. https://doi.org/10.1029/JB094iB05p05560.

Gravelle, R., McCay, R., 2007. [illegible] and structural styles in the Makran accretionary prism, offshore Iran. Sediment. Geol. 196, 157–179. https://doi.org/10.1016/j.sedgeo.2006.05.030.

Griffin, J., Latief, H., Kongko, W., Harig, S., Horspool, N., Hanung, R., Rojali, A., Maher, N., Fuchs, A., Hossen, J., Upi, S., Edi Dewanto, S., Rakowsky, N., Cummins, P., 2015. An evaluation of onshore digital elevation models for modeling tsunami inundation zones. Front. Earth Sci. 3, 1–16. https://doi.org/10.3389/feart.2015.00032.

Harbitz, C.B., Løvholt, F., Bungum, H., 2014. Submarine landslide tsunamis: How extreme and how likely? Nat. Hazards 72, 1341–1374. https://doi.org/10.1007/s11069-013-0681-3.

Hari, V., Sharath, A., [illegible], 2021. Dual response of Arabian Sea cyclones and strength of Indian monsoon to Southern Atlantic Ocean. Clim. Dyn. 56, 2149–2161. https://doi.org/10.1007/s00382-020-05577-6.

Heidarzadeh, M., Satake, K., 2014a. Possible sources of the tsunami observed in the northwestern Indian ocean following the 2013 September 24 Mw 7.7 Pakistan inland earthquake. Geophys. J. Int. 199, 752–766. https://doi.org/10.1093/gji/ggu297.

Heidarzadeh, M., Satake, K., 2014b. First Insights into the Source of the Makran Tsunami of 27 November 1945 from Tsunami Waveforms and Coastal Deformation Data. Pure Appl. Geophys. 172, 621–640. https://doi.org/10.1007/s00024-014-0948-y.

Heidarzadeh, M., Satake, K., 2017. A combined earthquake-landslide source model for the tsunami from the 27 November 1945 Mw 8.1 Makran earthquake. Bull. Seismol. Soc. Am. 107, 1033–1040. https://doi.org/10.1785/0120160196.

Heidarzadeh, M., Pirooz, M.D., Zaker, N.H., Mokhtari, M., 2007. Modeling of tsunami propagation in the vicinity of the southern coasts of Iran. Int. J. Civ. Eng. 5, 223–234. https://doi.org/[illegible].

Heidarzadeh, M., Pirooz, M.D., Zaker, N.H., Yalciner, A.C., Mokhtari, M., Esmaeily, A., 2008. Historical tsunami in the Makran Subduction Zone off the southern coasts of Iran and Pakistan and results of numerical modeling. Ocean Eng. 35, 774–786. https://doi.org/10.1016/j.oceaneng.2008.01.017.

Heidarzadeh, M., Pirooz, M.D., Zaker, N.H., 2009a. Modeling the near-field effects of the worst-case tsunami in the Makran subduction zone. Ocean Eng. 36, 368–376. https://doi.org/10.1016/j.oceaneng.2009.01.004.

Heidarzadeh, M., Pirooz, M.D., Zaker, N.H., Yalciner, A.C., 2009b. Preliminary estimation of the tsunami hazards associated with the Makran subduction zone at the northwestern Indian Ocean. Nat. Hazards 48, 229–243. https://doi.org/10.1007/s11069-008-9259-x.

Hoechner, A., Babeyko, A.Y., Zamora, N., 2016. Probabilistic tsunami hazard assessment for the Makran region with focus on maximum magnitude assumption. Nat. Hazards Earth Syst. Sci. 16, 1339–1350. https://doi.org/10.5194/nhess-16-1339-2016.

Hoffmann, G., Reicherter, K., 2014. Reconstructing Anthropocene extreme flood events by using their deposits. Z. Geomorphol. Suppl. Issues 58, 1–5. https://doi.org/[illegible].

Hoffmann, G., Reicherter, K., [illegible], 2013. [illegible] Tsunami Impact along the Coastline of Oman. [illegible].

Hoffmann, G., Rupprechter, M., Mahin, [illegible], 2013a. Block and boulder accumulations along the coastline between Fins and Sur (Sultanate of Oman): Tsunamigenic remains? Nat. Hazards 65, 851–873. https://doi.org/10.1007/s11069-012-0399-7.

Hoffmann, G., Rupprechter, M., Al Balushi, N., Grützner, C., Reicherter, K., 2013b. The impact of the 1945 Makran tsunami along the coastlines of the Arabian Sea (Northern Indian Ocean) – a review. Z. Geomorphol. Suppl. Issues 57, 257–277. https://doi.org/10.1127/0372-8854/2013/s-00134.

Hoffmann, G., Al-Yahyai, S., Naeem, G., Kociok, M., Grützner, C., 2014. An Indian Ocean tsunami triggered remotely by an onshore earthquake in Balochistan, Pakistan. Geology 42, 883–886. https://doi.org/10.1130/G35756.1.

Hoffmann, G., Grützner, C., Reicherter, K., Preusser, F., 2015. Geo-archaeological evidence for a Holocene extreme flooding event within the Arabian Sea (Ras al Hadd, Oman). Quat. Sci. Rev. 113, 123–133. https://doi.org/10.1016/j.quascirev.2014.09.031.

Hoffmann, G., Grützner, C., Schneider, B., Preusser, F., Reicherter, K., 2020. Large Holocene tsunamis in the northern Arabian Sea. Mar. Geol. 419, https://doi.org/10.1016/j.margeo.2019.106068.

Hosseini Ilkhchi, A., [illegible], 2018. Splay Faults in the Makran Subduction Zone and Dynamics of their Transform Coseismic Stress. [illegible]. https://doi.org/[illegible].

Jaiswal, R.K., Singh, A.P., Rastogi, B.K., 2009. Simulation of the Arabian Sea Tsunami propagation generated due to 1945 Makran Earthquake and its effect on western parts of Gujarat (India). Nat. Hazards 48, 245–258. https://doi.org/10.1007/s11069-008-9261-3.

Kakar, D.M., [illegible], Hoffmann, G., 2014. Balochistan [illegible] [illegible] Indian Ocean [illegible]. [illegible].

Kaur, S.K., Gupta, H., 2003. Success and failure of early warning systems: A case study of the Gujarat Cyclone of June 1998. In: Zschau, J., Küppers, A. (Eds.), Early Warning Systems for Natural Disaster Reduction. Springer, Berlin Heidelberg, pp. 189–202. https://doi.org/10.1007/978-3-642-55903-7_26.

Khaledzadeh, M., Ghods, A., 2022. Estimation of size of megathrust zone in the Makran subduction system by thermal modelling. Geophys. J. Int. 228, 1530–1540. https://doi.org/10.1093/gji/ggab417.

Khan, S.A., Shah, M.A., Qaisar, M., 2020a. Seismic risk analysis of coastal area of Pakistan. Acta Geophys. Sin. English Ed. 13, 282–294. https://doi.org/10.1007/s11589-020-00373-6.

Khan, S.A., Shah, M.A., Qaisar, M., 2020b. Seismic risk analysis of coastal area of Pakistan. Acta Geophys. Sin. English Ed. 13, 282. https://doi.org/10.1007/s11589-020-00373-6.

Khan, M.A., [illegible], 2008. Preliminary geodetic constraints on plate boundary deformation on the western edge of the Indian plate from TriGGnet (Tri-University GPS Geodesy Network). J. Himal. Earth Sci. 41, 71–87.

Knapp, K.R., Kruk, M.C., Levinson, D.H., Diamond, H.J., Neumann, C.J., 2010. The international best track archive for climate stewardship (IBTrACS). Bull. Am. Meteorol. Soc. 91, 363–376. https://doi.org/10.1175/2009BAMS2755.1.

Kopp, C., Fruehn, J., Flueh, E.R., Reichert, C., Kukowski, N., Bialas, J., Klaeschen, D., 2000. Structure of the makran subduction zone from wide-angle and reflection seismic data. Tectonophysics 329, 171–191. https://doi.org/10.1016/S0040-1951(00)00195-5.

Kuwayama, S., [illegible], 2014. The impact of the 2011 Tohoku earthquake tsunami disaster and implications to the reconstruction. Soils Found. 54, 560–572. https://doi.org/10.1016/j.sandf.2014.06.005.

Koster, B., Hoffmann, G., Grützner, C., Reicherter, K., 2014. Ground penetrating radar facies of inferred tsunami deposits on the shores of the Arabian Sea (Northern Indian Ocean). Mar. Geol. 351, 13–24. https://doi.org/10.1016/j.margeo.2014.03.002.

Kukowski, N., Schillhorn, T., Flueh, E.R., Huhn, K., 2000. Newly identified strike-slip plate boundary in the northeastern Arabian Sea. Geology 28, 355–358.

Kukowski, N., Schillhorn, T., Huhn, K., von Rad, U., Husen, S., Flueh, E.R., 2001. Morphotectonics and mechanics of the central Makran accretionary wedge off Pakistan. Mar. Geol. 173, 1–19. https://doi.org/10.1016/S0025-3227(00)00167-5.

Laane, J.L., Chen, W.-P., 1989. The Makran earthquake of 1983 April 18: a possible analogue to the Puget Sound earthquake of 1965. Geophys. J. Int. 98, 1–9.

Latcharote, P., Al-Salem, K., Suppasri, A., Pokavanich, T., Toda, S., Jayaramu, Y., Al-Enezi, A., Al-Ragum, A., Imamura, F., Ammari, K.A., 2018. Tsunami hazard evaluation for Kuwait and Arabian Gulf due to Makran Subduction Zone and Subaerial landslides. Nat. Hazards 93, 127–152. https://doi.org/10.1007/s11069-017-3087-7.

Liu, P.L.-F., Cho, Y.S., Yoon, S.B., Seo, S.N., 1995. Numerical Simulations of the 1960 Chilean Tsunami Propagation and Inundation at Hilo, Hawaii, pp. 99–115. https://doi.org/10.1007/978-94-015-8565-1_8.

Løvholt, F., 2017. Tsunami Hazard and Risk Assessment. [illegible] Risk [illegible], pp. 1–8.

[illegible], 2012. Mapping of Tsunami Hazard along Makran Coast of Pakistan, 1–20.

[illegible], 2012. Tsunami Vulnerability Function Development Based on the 2011 Tohoku Earthquake in Japan. In: 15 World Conf. Earthq. Eng.

Milliman, J.D., Syvitski, J.P.M., 1992. Geomorphic/tectonic control of sediment discharge to the ocean: the importance of small mountainous rivers. J. Geol. 100, 525–544. https://doi.org/10.1086/629606.

[illegible], 2014. On the use of Green's summation for tsunami waveform estimation: a case study. Geophys. J. Int. 199, 480–494. https://doi.org/10.1093/gji/ggu268.

Mouchot, N., Loncke, L., Mahieux, G., Bourget, J., Lallemant, S., Ellouz-Zimmermann, N., Leturmy, P., 2010. Recent sedimentary processes along the Makran trench (Makran active margin, off Pakistan). Mar. Geol. 271, 17–31. https://doi.org/10.1016/j.margeo.2010.01.006.

Murty, T.S., 1984. Storm surges-meteorological ocean tides. Can. Bull. Fish. Aquat. Sci. Fisheries and Oceans Canada, p. 897.

Neetu, S., Suresh, I., Shankar, R., Nagarajan, B., Sharma, R., Shenoi, S.S.C., Unnikrishnan, A.S., Sundar, D., 2011. Trapped waves of the 27 November 1945 Makran tsunami: Observations and numerical modeling. Nat. Hazards 59, 1609–1618. https://doi.org/10.1007/s11069-011-9854-0.

Okal, E.A., Synolakis, C.E., 2008. Far-field tsunami hazard from mega-thrust earthquakes in the Indian Ocean. Geophys. J. Int. 172, 995–1015. https://doi.org/10.1111/j.1365-246X.2007.03674.x.

Page, W.D., Alt, J.N., Cluff, L.S., Plafker, G., 1979. Evidence for the recurrence of large-magnitude earthquakes along the Makran coast of Iran and Pakistan. Tectonophysics 52, 533–547. https://doi.org/10.1016/0040-1951(79)90269-5.

Pagnoni, G., Armigliato, A., Tinti, S., 2021. Estimation of human damage and economic loss of buildings related to tsunami inundation in the city of Augusta, Italy. Geol. Soc. Spec. Publ. 501, 327–340. https://doi.org/10.1144/SP501-2019-124.

Payande, A.R., Niksokhan, M.H., Naserian, H., 2015. Tsunami hazard assessment of Chabahar bay related to megathrust seismogenic potential of the Makran subduction zone. Nat. Hazards 76, 161–176. https://doi.org/10.1007/s11069-014-1478-x.

Pedgley, D.E., 1969. Cyclones along the Arabian Coast. Weather.

Pendse, C.G., 1946. The Makran Earthquake of the 28th November 1945. Sci. Notes 10, 141–145.

Pilarczyk, J.E., Reinhardt, E.G., 2012. Testing foraminiferal taphonomy as a tsunami indicator in a shallow arid system lagoon: Sur, Sultanate of Oman. Mar. Geol. 295–298, 128–136. https://doi.org/10.1016/j.margeo.2011.12.002.

Pilarczyk, J.E., Reinhardt, E.G., Boyce, J.I., Schwarcz, H.P., Donato, S.V., 2011. Assessing surficial foraminiferal distributions as an overwash indicator in Sur Lagoon, Sultanate of Oman. Mar. Micropaleontol. 80, 62–73. https://doi.org/10.1016/j.marmicro.2011.06.001.

Platt, J.P., Leggett, J.K., Young, J., Raza, H., Alam, S., 1985. Large-scale sediment underplating in the Makran accretionary prism, southwest Pakistan. Geology 13, 507–511. https://doi.org/10.1130/0091-7613(1985)13<507:LSUITM>2.0.CO;2.

Prasetya, G., Beavan, J., de Lange, W., Black, K., Healy, T., 2011. Mapping of inundation dynamics on Banda Aceh, Indonesia during the great Sumatra tsunami December 26, 2004. Nat. Hazards 58, 1029–1055. https://doi.org/10.1007/s11069-010-9710-[illegible].

Prins, M.A., Postma, G., Cleveringa, J., Cramp, A., Kenyon, N.H., 2000. Controls on terrigenous sediment supply to the Arabian Sea during the late Quaternary: The Indus Fan. Mar. Geol. 169, 327–349. https://doi.org/10.1016/S0025-3227(00)00086-4.

Prizomwala, S.P., Gandhi, D., Ukey, V.M., Bhatt, N., Rastogi, B.K., 2015. Coastal boulders as evidences of high-energy marine events from Diu Island, west coast of India: storm or palaeotsunami? Nat. Hazards 75, 1187–1203. https://doi.org/10.1007/s11069-014-1371-8.

Prizomwala, S.P., Gandhi, D., Bhatt, N., Winkler, W., Kumar, M.R., Makwana, N., Bhatt, N., 2018. Geological evidence for AD 1008 tsunami along the Kachchh coast, Western India: Implications for hazard along the Makran Subduction Zone. Sci. Rep. 8, 1–8. https://doi.org/10.1038/s41598-018-35193-x.

Prizomwala, S.P., Tandon, A., Joshi, N., Makwana, N., 2021. Reconstructing the catalogue for extreme wave events from the Gujarat coastline (Western India) and their implications on coastal geology during the last 6000 years. Quat. Int. 599–600, 24–31. https://doi.org/10.1016/j.quaint.2020.08.034.

Prizomwala, S.P., [illegible], Tandon, A., Das, A., Makwana, N., Joshi, N., 2022. Geological footprints of the 1945 Makran tsunami from the west coast of India. Mar. Geol. 444, 106775. https://doi.org/10.1016/j.margeo.2022.106775.

Quittmeyer, R.C., Kafka, A.L., 1984. Constraints on plate motions in southern Pakistan and the northern Arabian Sea from the focal mechanisms of small earthquakes. J. Geophys. Res. 89, 2444–2458.

Quittmeyer, R.C., Farah, A., Jacob, K.H., 1979. The seismicity of Pakistan and its relation to surface faults. In: Farah, A., DeJong, K.A. (Eds.), Geodynamics of Pakistan. Geological Survey of Pakistan, Quetta, pp. 271–284.

Rafi, Z., Mahmood, N., 2010. Tsunami Simulation for Historic Earthquake at Makran Subduction Zone. Sci. Tech. Dev. [illegible].

Rajendran, C.P., Ramanamurthy, M.V., Reddy, N.T., Rajendran, K., 2008. Hazard implications of the late arrival of the 1945 Makran tsunami. Curr. Sci. 95, 1739–1743.

[illegible], 2021. The Orphan Tsunami of 1524 on the Konkan Coast, Western India, and Its Implications. Pure Appl. Geophys. https://doi.org/10.1007/s00024-020-02579-5.

Rashidi, A., Shomali, Z.H., Dutykh, D., Keshavarz Farajkhah, N., 2018a. Evaluation of tsunami wave energy generated by earthquakes in the Makran subduction zone. Ocean Eng. 165, 131–139. https://doi.org/10.1016/j.oceaneng.2018.07.027.

Rashidi, A., Shomali, Z.H., Keshavarz Farajkhah, N., 2018b. Tsunami simulations in the Western Makran using hypothetical heterogeneous source models from World's Great Earthquakes. Pure Appl. Geophys. 175, 1325–1340. https://doi.org/10.1007/s00024-018-1842-x.

Rashidi, A., Shomali, Z.H., Dutykh, D., Keshavarz Farajkhah, N., 2020. Tsunami hazard assessment in the Makran subduction zone. Nat. Hazards 100, 861–875. https://doi.org/10.1007/s11069-019-03848-z.

Rastgoftar, E., Soltanpour, M., 2016. Study and numerical modeling of 1945 Makran tsunami due to a probable submarine landslide. Nat. Hazards 83, 929–945. https://doi.org/10.1007/s11069-016-2356-1.

Rehman, K., [illegible], 2013. [illegible]. J. Earthq. Eng. [illegible].

Reilinger, R., McClusky, S., Vernant, P., Lawrence, S., Ergintav, S., Cakmak, R., Ozener, H., Kadirov, F., Guliev, I., Stepanyan, R., Nadariya, M., Hahubia, G., Mahmoud, S., Sakr, K., ArRajehi, A., Paradissis, D., Al-Aydrus, A., Prilepin, M., Guseva, T., Evren, E., Dmitrotsa, A., Filikov, S.V., Gomez, F., Al-Ghazzi, R., Karam, G., 2006. GPS constraints on continental deformation in the Africa-Arabia-Eurasia continental collision zone and implications for the dynamics of plate interactions. J. Geophys. Res. Solid Earth 111, 1–26. https://doi.org/10.1029/2005JB004051.

Röbke, B.R., Vött, A., Willershäuser, T., Fischer, P., Hadler, H., 2013. Considering tsunami palaeogeographical changes in a numerical tsunami model – A prognostic basis to compare simulation results with field traces from historic tsunami landings in western Greece. Z. Geomorphol. 57, 137–158. https://doi.org/10.1127/0372-8854/2013/S-00112.

Röbke, B.R., Schüttrumpf, H., Vött, A., 2016. Effects of different boundary conditions and palaeotopographies on the onshore response of tsunamis in a numerical model – A case study from western Greece. Cont. Shelf Res. 124, 182–199. https://doi.org/10.1016/j.csr.2016.04.010.

Röbke, B.R., Schüttrumpf, H., Vött, A., 2018. Hydro- and morphodynamic tsunami simulations for the Ambrakian Gulf (Greece) and comparison with geoscientific field traces. Geophys. J. Int. 213, 217–[illegible]. https://doi.org/10.1093/gji/ggx553.

Rodriguez, M., Fournier, M., Chamot-Rooke, N., Huchon, P., Bourget, J., Sorbier, M., Zaragosi, S., Rabaute, A., 2011. Neotectonics of the Owen Fracture Zone (NW Indian Ocean): Structural evolution of an oceanic strike-slip plate boundary. Geochem. Geophys. Geosyst. 12. https://doi.org/10.1029/2011GC003731.

Rodriguez, M., Fournier, M., Chamot-Rooke, N., Huchon, P., Zaragosi, S., Rabaute, A., 2012. Mass wasting processes along the Owen Ridge (Northwest Indian Ocean). Mar. Geol. 326–328, 80–100. https://doi.org/10.1016/j.margeo.2012.08.008.

Rodriguez, M., Chamot-Rooke, N., Hébert, H., Fournier, M., Huchon, P., 2013. Owen Ridge deep-water submarine landslides: implications for tsunami hazard along the Oman coast. Nat. Hazards Earth Syst. Sci. 13, 417–424. https://doi.org/10.5194/nhess-13-417-2013.

[illegible], 2012. Tsunami simulation along the south west coast of India [illegible]. Indian J. Geo-Marine Sci. 41, [illegible].

Salaree, A., Okal, E.A., 2015. Field survey and modelling of the Caspian Sea tsunami of 1990 June 20. Geophys. J. Int. 201, 621–639. https://doi.org/10.1093/gji/ggv044.

Salmanidou, D.M., Heidarzadeh, M., Guillas, S., 2019. Probabilistic Landslide-Generated Tsunamis in the Indus Canyon, NW Indian Ocean, Using Statistical Emulation. Pure Appl. Geophys. 176, 3099–3114. https://doi.org/10.1007/s00024-019-02187-3.

Sangode, S.J., Meshram, D.C., 2013. A comparative study on the style of palaeotsunami deposits at two sites on the west coast of India. Nat. Hazards 66, 403–432. https://doi.org/10.1007/s11069-012-0492-9.

Sarker, M.A., 2018. Numerical modelling of tsunami in the Makran Subduction Zone – A case study on the 1945 event. J. Oper. Oceanogr. 11, [illegible]. https://doi.org/10.1080/1755876X.2018.1527883.

Saunders, M.A., Lea, A.S., 2008. Large contribution of sea surface warming to recent increase in Atlantic hurricane activity. Nature 451, 557–560. https://doi.org/10.1038/nature06422.

Schneider, B., Hoffmann, G., Reicherter, K., 2016. Scenario-based tsunami risk assessment using a static flooding approach and high-resolution digital elevation data: An example from Muscat in Oman. Glob. Planet. Chang. 139, 183–194. https://doi.org/10.1016/j.gloplacha.2016.02.005.

Shah-Hosseini, M., Morhange, C., Naderi Beni, A., Marriner, N., Lahijani, H., Hamzeh, M., Sabatier, F., 2011. Coastal boulders as evidence for high-energy waves on the Iranian coast of Makran. Mar. Geol. 290, 17–28. https://doi.org/10.1016/j.margeo.2011.10.003.

Singh, V.K., Roxy, M.K., 2022. A review of ocean-atmosphere interactions during tropical cyclones in the north Indian Ocean. Earth-Sci. Rev. 226, 103967. https://doi.org/10.1016/j.earscirev.2022.103967.

Singh, V.K., Roxy, M.K., Deshpande, M., 2020. The unusual long track and rapid intensification of very severe cyclone Ockhi. Curr. Sci. 119, 771–779. https://doi.org/10.18520/cs/v119/i5/771-779.

Smart, G.M., Crowley, K.H.M., Lane, E.M., 2016. Estimating tsunami run-up. Nat. Hazards 80, 1933–1947. https://doi.org/10.1007/s11069-015-2033-4.

Smith, G.L., McNeill, L., Henstock, T.J., Bull, J., 2012. The structure and fault activity of the Makran accretionary prism. J. Geophys. Res. 117, 1–17. https://doi.org/10.1029/2012JB009312.

Smith, G.L., McNeill, L.C., Wang, K.M., He, Jiangheng, Henstock, T.J., 2013. Thermal structure and megathrust seismogenic potential of the Makran subduction zone. Geophys. Res. Lett. 40, 1528–1533. https://doi.org/10.1002/grl.50374.

[illegible], 2011. [illegible]. [illegible] 40, [illegible].

[illegible], A., [illegible], F., [illegible], T., [illegible], [illegible], 2016. Tsunami Hazard Assessment for the Arabian Gulf from Earthquakes and Surface Landslides. J. Japan Soc. Civ. Eng. Ser. B2. https://doi.org/10.2208/kaigan.72.I_1675. Coastal Eng. 72, I_1675–I_1680.

[illegible], [illegible], 2014. Effect of Murray ridge on the tsunami propagation from Makran subduction zone. Geophys. J. Int. 199, 1430–1441. https://doi.org/10.1093/gji/ggu333.

Tarbotton, C., Dominey-Howes, D., Goff, J.R., Papathoma-Köhle, M., Dall'Osso, F., Turner, I.L., 2012. GIS-based techniques for assessing the vulnerability of buildings to tsunami: current approaches and future steps. Geol. Soc. Spec. Publ. 361, 115–125. https://doi.org/10.1144/SP361.10.

[illegible], S.M., [illegible], [illegible], 2016. Coastal [illegible] from the Iranian coast of Makran: [illegible] Bay to [illegible] Bay as an indicator of tsunamis. In: Geological Society of America Annual Meeting, Denver, Colorado, pp. 42–62. https://doi.org/10.1130/abs/2016AM-[illegible].

Vernant, P., Nilforoushan, F., Hatzfeld, D., Abbassi, M.R., Vigny, C., Masson, F., Nankali, H., Martinod, J., Ashtiani, A., Bayer, R., Tavakoli, F., Chéry, J., 2004. Present-day crustal deformation and plate kinematics in the Middle East constrained by GPS measurements in Iran and northern Oman. Geophys. J. Int. 157, 381–398. https://doi.org/10.1111/j.1365-246X.2004.02222.x.

Waseem, M., Khan, M.A., Khan, S., 2019. Seismic sources for southern Pakistan and seismic hazard assessment of Karachi. Nat. Hazards 99, 511–536. https://doi.org/10.1007/s11069-019-[illegible].

Waseem, M., Khan, S., Asif Khan, M., 2020. Probabilistic Seismic Hazard Assessment of Pakistan Territory Using an Areal Source Model. Pure Appl. Geophys. 177, 3577–3597. https://doi.org/10.1007/s00024-020-[illegible].

White, R.S., Louden, K.E., 1982. The Makran Continental Margin: Structure of a Thickly Sedimented Convergent Plate Boundary. Convergent Margins: Field Investigations of Margin Structure and Stratigraphy.

Williams, J., Paris, R., [illegible], [illegible], [illegible], 2021. [illegible] quantification of tsunami hazard [illegible] in a [illegible] small island developing state: the case of [illegible]. [illegible]. https://doi.org/[illegible].

Yanagisawa, H., [illegible], 2008. Tsunami hazard assessment along the coast of Pakistan based on the 1945 Makran tsunami. J. Jpn. Soc. Civ. Eng. Ser. B2. https://doi.org/10.2208/[illegible]. Coastal Eng. [illegible].

Yang, X., [illegible], 2022. [illegible] of the 2017 Mw6.3 [illegible] earthquake and its significance for future major earthquakes in the eastern Makran. Geophys. J. Int. 231, 1424–1440. https://doi.org/10.1093/gji/[illegible].

Zafarani, H., [illegible], 2022. Probabilistic tsunami hazard analysis for western Makran. Natural Hazards. Springer, Netherlands. https://doi.org/10.1007/s11069-[illegible].

Zhang, W., Villarini, G., 2019. On the role of the Atlantic Ocean in forcing tropical cyclones in the Arabian Sea. Atmos. Res. [illegible]. https://doi.org/10.1016/j.atmosres.2019.[illegible].